7-1-2011

Hydraulic and geospatial analyses of stream engineering and habitat restoration near Los Lunas, NM

Stephen Kissock

Stephen Kissock

Candidate

CIVIL ENGINEERING

Department

This thesis is approved, and it is acceptable in quality and form for publication:

Approved by the Thesis Committee:

Dr. Julie Coonrod, Chairperson

Dr. Bruce Thomson

Dr. Mark Stone

Dr. Tim J. Ward

Accepted:

Dean, Graduate School

Date

HYDRAULIC AND GEOSPATIAL ANALYSES OF STREAM ENGINEERING AND HABITAT RESTORATION NEAR LOS LUNAS, NEW MEXICO

BY

STEPHEN KISSOCK

B.S., ENVIRONMENTAL SCIENCE
OREGON STATE UNIVERSITY, 2004

THESIS

Submitted in Partial Fulfillment of the
Requirements for the Degree of

Master of Science
Civil Engineering

The University of New Mexico
Albuquerque, New Mexico

May, 2011

DEDICATION

I heartily dedicate this body of work to my wife Amanda who never let me complain about work for more than five minutes. I also dedicate this to my daughter Arden born during the final stages of this project and who will likely find it all very dull.

ACKNOWLEDGEMENTS

I heartily acknowledge the instruction and guidance of my graduate advisor and committee chair, Dr. Julie Coonrod, and my entire thesis committee including Dr. Bruce Thomson, Dr. Mark Stone, and Dr. Tim Ward. I also acknowledge Dr. Mick Porter for his insight and guidance through the entire process from thesis proposal to completion. I also greatly thank Dr. Robert Dudley and Dr. Steven Platania for their sharing and explanation of data without which this habitat mapping project would be incomplete. I thank Anders Lundahl for his candid conversation of the use of the 2008 LiDAR in hydraulic modeling by the State of New Mexico. I also thank Donald Gallegos for his knowledgeable comments on the regulated hydrology in the Middle Rio Grande. I also extend my thanks to Cameron Ackerman who provided significant assistance with troubleshooting of the hydraulic model. I greatly appreciate Susan Bittick for providing funding through the U.S. Army Corps of Engineers. And last but not least, to April Fitzner and Dennis Garcia for allowing time to integrate this project into my work schedule.

HYDRAULIC AND GEOSPATIAL ANALYSES OF STREAM ENGINEERING AND HABITAT RESTORATION NEAR LOS LUNAS, NEW MEXICO

BY

STEPHEN KISSOCK

ABSTRACT OF THESIS

Submitted in Partial Fulfillment of the
Requirements for the Degree of

Master of Science
Civil Engineering

The University of New Mexico
Albuquerque, New Mexico

May, 2011

HYDRAULIC AND GEOSPATIAL ANALYSES OF STREAM ENGINEERING AND HABITAT RESTORATION NEAR LOS LUNAS, NEW MEXICO

Stephen Kissock

Bachelor of Science, Environmental Science
Oregon State University, 2004

Master of Science, Civil Engineering
University of New Mexico, 2011

ABSTRACT

Stream restoration is a complex process encompassing multiple disciplines and organizations to achieve specific, immediate and long-term goals. Analyses of many completed projects are limited to narrow objectives that commonly exclude the same broad scopes envisioned during the planning process. This thesis studies one completed habitat restoration project in terms of its engineering and biological sustainability using geospatial analysis procedures not widely applied to these goals. These procedures include adjustment of a digital terrain model for hydraulic accuracy, the use of the digital terrain model and aerial imagery for the digitization of features used in hydraulic modeling, and the geospatial analyses of the resulting hydraulic model parameters of depth, velocity, and shear stress to map habitat preferences and discuss sustainability. Methods presented here have application to a broad range of habitat restoration projects, from project planning stages to post-completion monitoring.

The Los Lunas Habitat Restoration site was began when a fire decimated the riparian vegetation in the area, opening the door to the site being overtaken by non-native and invasive species proliferating in the area. The goals of the project were to construct

habitat preferential to the endangered species, the Rio Grande silvery minnow (*Hybognathus amarus*) and the Southwestern willow flycatcher (*Empidonax traillii extimus*), by restoring a natural inundation regime to the overbank area. This inundation regime provides spawning and rearing habitat for the minnow in addition to promoting native vegetation over non-native and invasive vegetation.

To evaluate the success of the project, hydraulic modeling and geospatial analysis procedures are undertaken using the most current digital terrain model (collected using LiDAR), a readily available hydraulic modeling software package (HEC-RAS), and the frontrunner of geographic information systems (ArcMap). Features used in hydraulic modeling were manually digitized in most cases although some were assisted using the spatial extent of the LiDAR point cloud. Data exchange between HEC-RAS and ArcMap allowed iterative refinement of the hydraulic model and detailed investigation of results. This detailed spatial investigation is a novel approach to the analysis of a hydraulic model for biological functionality and sustainability of the site.

The site shows expansive areas of habitat characterized with the maximum frequency of use by the targeted species. The sediment balance includes both erosion and deposition, but the tendency towards erosion necessitates some maintenance of the project in the future. The reinstatement of a natural inundation regime at the project site shows long-term establishment of native vegetation, which the flycatcher prefers and which is capable of outcompeting invasive and non-native vegetation species. This study concludes that the site is sustainable by continuing to provide habitat to the endangered species targeted for habitat restoration.

Table of Contents

List of Figures

List of Tables

The Middle Rio Grande

Background

The Rio Grande has been populated and utilized for agriculture for thousands of years, first by American Indians, then Spanish colonials, Mexicans, and most recently Americans (Simmons, 1988). In New Mexico, the narrow strip of arable, riparian woodland adjacent to the Rio Grande is a sanctuary from the hot and arid landscape pervasive in the state. This riparian woodland is referred to as the bosque, the Spanish word for forest. While the vast majority of the Middle Rio Grande semi-arid grasslands receive only 10 inches of rain per year (New Mexico State University, 2010), the proximity to the Rio Grande allows agricultural irrigation and proliferation of the bosque.

The history of stream management in the southwestern United States is dominated by channelization and regulation until the last decade of the 20th Century. Streams were routinely tapped for irrigation, dammed for flow regulation, confined with levees for flood protection and littered with structures such as jetty jacks to reinforce straightening and channelization. Streams were engineered to accomplish specific regulatory goals within the ethos of the time, which did not include environmental considerations. Unfortunately, environmental degradation became rampant before the ethos shifted and numerous species across the southwestern United States became threatened or endangered. Ultimately, legislation was enacted to manage environmental resources exclusively for listed species.

Restoring streams for habitat quality commonly involves designing structures and topography to induce certain hydrologic conditions and a desired biological system, such

as designing depressions with inflow and outflow carefully engineered to build wetland habitat. Hydraulic modeling allows quantification of the sustainability of the wetland hydrology. Model results show the water surface elevation, extent of inundation and several other characteristics of the flow including the depth, velocity and shear stress acting on the channel. Within a geographic information system (GIS) environment these results can be mapped and coupled with indicators of habitat quality to visually interpret the affects of hydraulics on habitat. Spatial statistics performed within a GIS show areas of clustering or dispersal, quantifying the distribution of quality habitat. This correlation of hydraulics to habitat quality makes hydraulic engineering a powerful tool in stream restoration.

Study Area

As seen in Figure 1, the Village of Los Lunas, New Mexico is located in Valencia County approximately 25 miles south of Albuquerque. Agricultural organization in the 1930s under the Middle Rio Grande Conservancy District (MRGCD) drained what had been mainly swampland in the Los Lunas area while installing drains, irrigation canals and levees (FEMA, 2010). In the early 1950s, the Middle Rio Grande began to be modified by the Bureau of Reclamation for the purposes of maintaining channel capacity and stabilizing the river channel (Scurlock, 1998). Kellner jetty jacks were installed to "stabilize the river channel and protect the levees" (Scurlock, 1998, p. 282). These are structures comprised of three 16-foot steel beams bolted at their centers and laced with steel cable. During floods, these heavy structures remain relatively stable while debris and sediment become trapped within the lattice of steel wire.

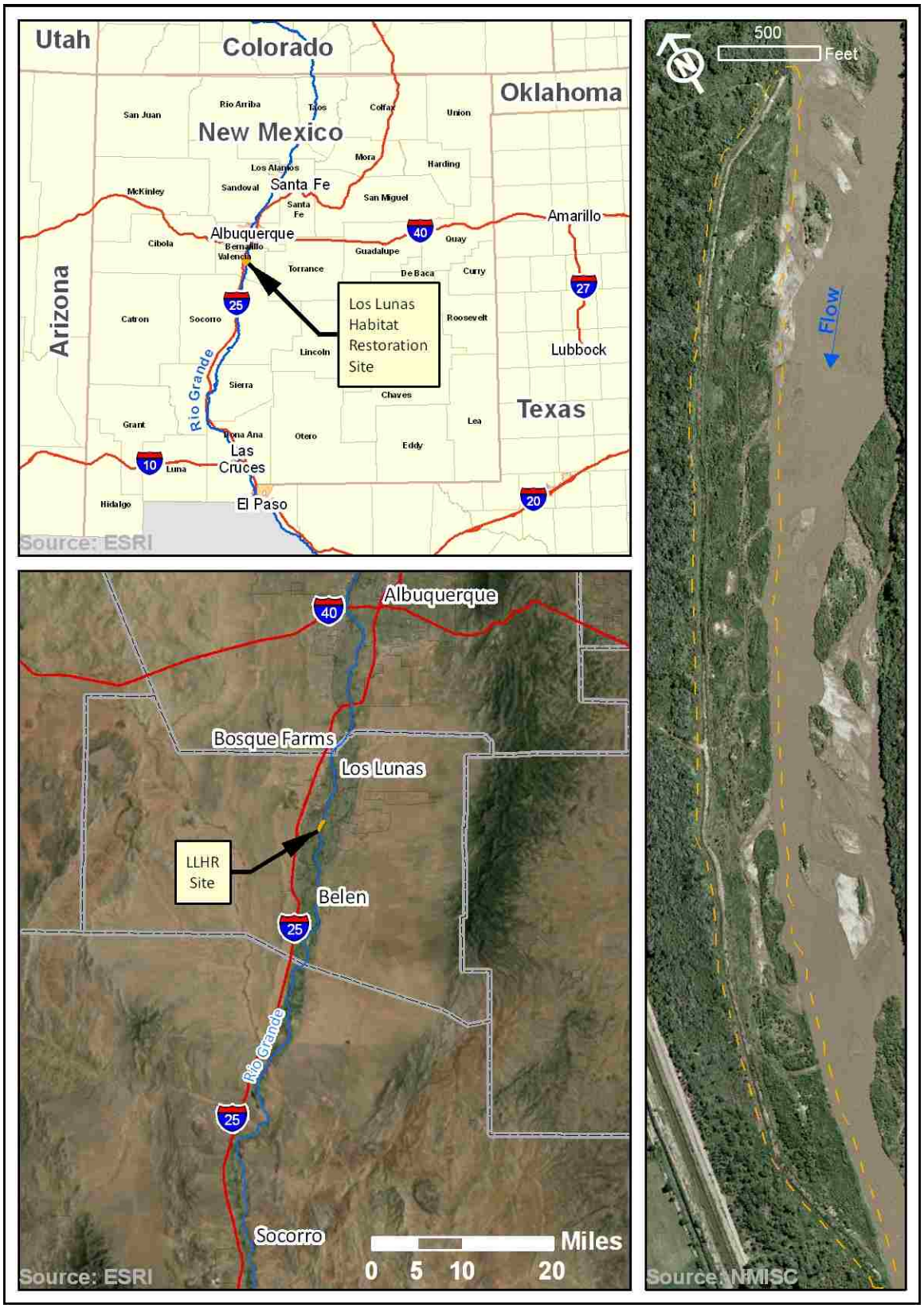

Figure 1: Vicinity Map of the Los Lunas Habitat Restoration site (orange line)

The Los Lunas Habitat Restoration Site is a joint project between the U.S. Army Corps of Engineers (USACE), the U.S. Bureau of Reclamation (USBR), and the MRGCD. It was undertaken as a response to the June 2001 Biological Opinion (BO) from the USFWS as part of a larger Middle Rio Grande habitat restoration initiative to improve habitat for the silvery minnow (*Hybognathus amarus*) and the southwest willow flycatcher (*Empidonax traillii extimus*) which were listed as endangered in 1994 and 1995, respectively. This site is approximately 3 miles south of the Village of Los Lunas proper, as seen in Figure 1. It burned in April 2000 destroying much of the vegetation and was then quickly colonized by invasive species such as saltcedar (*Tamarix* spp.) and Russian olive (*Eleagnus angustifolia*) (Siegle & Reed, 2007). This fire event provided a unique opportunity to design a restoration project with specific hydrologic, hydraulic and biological goals. These goals were based on known habitat quality parameters for both the minnow and flycatcher, including sufficient variations in stream bed profiles to provide areas of inundation and low velocities. Recolonization of the site by native species such as Rio Grande cottonwood (*Populus deltoids wislizenii*), coyote willow (*Salix exigua*), and Gooddings willow (*Salix gooddingii*) is an indirect goal facilitated by the reestablishment of an inundation regime.

The Middle Rio Grande has been surveyed by the Bureau of Reclamation at specific rangeline locations over time. Topographical surveys using Light Detection and Ranging (LiDAR) equipment were completed in 2008 and 2010. The LiDAR surveys generate a continuous topographical surface and are currently the highest resolution topography for hydraulic modeling.

Objective and approach

The objective of this proposed study is to develop a better understanding of the hydraulic conditions of the Los Lunas Habitat Restoration (LLHR) site located on the Middle Rio Grande south of Albuquerque with the overall goal to assist in management and recovery of endangered species. This objective will be met by a detailed hydraulic analysis of the stream restoration activities at the LLHR site including site characterization, geospatial analysis, and hydraulic modeling. The hydraulic modeling includes a quantification and spatial distribution of depth, velocity, and shear stress. The analysis includes the stability of instream sand bars, inundation characteristics of transverse channels, low velocity side channels, and overbank areas. Each component is analyzed in relation to the habitat needs and potential success of the minnow, flycatcher, and native vegetation species.

This study demonstrates a novel approach to the analysis of stream habitat restoration using interdisciplinary analysis based in the fields of hydraulic engineering, geography, and biology. The approach predicts habitat distribution in the case of proposed projects, is repeatable over time for the continued monitoring of completed projects, and is applicable to a wide variety of stream habitat restoration projects.

The study results include site characteristics, mapping of inundated areas, hydraulics of the Rio Grande at the LLHR site, and current status of the engineered features. Mapping of the inundated areas based on designed flows and engineered features are provided as raster data in Environmental Systems Research Institute (ESRI) grid format and georeferenced tagged image file format (GeoTIFF). Mapping of inundated areas includes depth and velocity of flow within engineered features and is

extended in relation to endangered species habitat quality. The instream sand bars, inundation characteristics of transverse channels, low velocity side channels, and overbank areas will be evaluated for overall change after installation and discussed in terms of hydraulic stability.

Hydraulic analysis of the LLHR site utilizes software from the USACE Hydrologic Engineering Center (HEC) called River Analysis System (HEC-RAS), a one dimensional hydraulic modeling software package. This software is used in conjunction with its geospatial counterpart, HEC-GeoRAS, within ArcMap. Spatial data such as stream centerlines and levees are digitized in the ArcMap GIS environment using imagery and terrain data, then exported into HEC-RAS format. This process is efficient in generating cross section geometric data necessary for HEC-RAS such as reach lengths, bank stations and coefficients of contraction and expansion. Local U.S. Geological Survey (USGS) stream gage data and engineering design specifications are used as input into a steady flow analysis in HEC-RAS.

Literature Review

Hydrology

The Rio Grande headwaters lie within the southern tip of the Rocky Mountain Range. The San Juan Mountains of southern Colorado and northern New Mexico are the primary source of snow melt runoff to the Rio Grande with additional contributions from the Jemez Mountains in New Mexico and the Sangre de Cristo Mountains spanning Colorado and New Mexico. The Continental Divide forms the western boundary of the Rio Grande Basin. A large area along the eastern side of the San Luis Valley in southern Colorado is considered noncontributing.

The main tributary to the Rio Grande is the Rio Chama which joins the Rio Grande above Cochiti Dam and is regulated, in downstream order, by Heron, El Vado and Abiquiu Dams. The Rio Chama also contributes water diverted from the headwaters of the San Juan Basin through the Azotea Tunnel beneath the Continental Divide into Willow Creek above Heron Reservoir. Other major Rio Grande tributaries include the Rio Pueblo de Taos, Jemez River, Galisteo Creek, Santa Fe River, Rio Salado, and Rio Puerco. Jemez Canyon and Galisteo Dams regulate the tributary flow only for flood control. Other dams for irrigation and water supply include Nichols and McClure Dams on the Santa Fe River, Santa Cruz Dam above the village of Chimayo, and the Nambe Falls Dam above Pojoaque Pueblo.

Generally speaking the term Middle Rio Grande incorporates the Rio Grande and its tributaries from downstream of Cochiti Dam north of Albuquerque to Elephant Butte Reservoir near Truth or Consequences, New Mexico (Scurlock, 1998). Cochiti Dam

regulates the flow for flood control in the Middle Rio Grande with one major municipal and three agricultural diversions influencing hydrology. The Upper Rio Grande spans southern Colorado and northern New Mexico comprising the Conejos River, the Rio Chama and the majority of the Sangre de Cristo streams (Scurlock, 1998). The dams in the Upper Rio Grande are mainly for irrigation storage and include Continental, Rio Grande, Santa Maria, and Platoro Dams. The Lower Rio Grande includes the reach from Elephant Butte and Caballo Reservoirs in southern New Mexico then along the international border between Mexico and the United States into the Gulf of Mexico.

Middle Rio Grande flows in the winter months from November to February are generally higher as Cochiti Dam makes releases to prepare for the spring runoff volume (D. Gallegos, personal communication, October 6, 2010). The spring runoff months of March, April, May, and June produce higher flows which are regulated by Cochiti Dam. Flows in the months between July and October are typically much lower after the snowmelt runoff season has ended and the Rio Grande is diverted for agricultural purposes (D. Gallegos, personal communication, October 6, 2010). Monsoon thunderstorms during the summer months can produce high spikes in stream flow for short periods of time.

One of the oldest USGS stream gages in the United States is located in New Mexico on the Rio Grande at the Otowi Bridge (now State Highway 502) near San Ildefonso in Santa Fe County. The gage, USGS 08313000 Rio Grande at Otowi Bridge near San Ildefonso, NM, began collecting data in February of 1895 with an interruption from December 1905 to June 1909 (USGS, 2010a). This gage is used as an index gage to assess the hydrology of the Middle Rio Grande in legal water deliveries within the state

of New Mexico and between Colorado, New Mexico and Texas as specified in the Rio Grande Compact (New Mexico Office of the State Engineer, 2010). The largest flood "since at least 1884 and probably since 1741" (USGS, 2010a, p 1) occurred here on May 23, 1920, with a peak of approximately 24,400 cubic feet per second (cfs), 629 cubic meters per second (cms), followed by the second highest peak on May 16, 1941, with 22,000 cfs (623 cms) (USGS, 2010a). The highest daily mean flow occurred on May 11, 1985, with 12,000 cfs (USGS, 2010a). The lowest daily mean was 195 cfs on August 4, 1977, and the lowest seven-day minimum was 229 on September 11, 1971 (USGS, 2010a). The 10 percent exceedance flow for the water years from 1971 to 2009 is 3,380 cfs (95.7 cms) (USGS, 2010a).

The hydrology of the LLHR site is analogous to that at Otowi. Flows at Otowi are regulated by several reservoirs including Abiquiu, El Vado and Heron and water is used for small-scale agricultural diversions. Flows at the LLHR site are regulated by Cochiti Dam, Jemez Canyon Dam and Galisteo Dam. The major difference in flows between Otowi and the LLHR is caused by the operation of Cochiti Dam, two larger agricultural diversions north and south of Albuquerque, and the Albuquerque municipal diversion. The LLHR site is flanked by irrigation canals on either side of the Rio Grande, with a diversion site upstream at Isleta Pueblo and return flows from the Peralta Wasteway downstream of the site.

The nearest gage station to the LLHR site is USGS 08331160 Rio Grande near Bosque Farms, NM, installed and maintained by the USGS. This gage has a period of record from March 16, 2006, to present and is located approximately 7.5 river miles upstream of the LLHR site (USGS, 2010f). The maximum daily value was on May 25,

2008, with 5,230 cfs recorded (USGS, 2010e). The minimum flows are also dramatically different with the lowest daily mean on October 26, 2006, with 15 cfs recorded and the lowest seven-day mean on September 11, 2007, with 23 cfs recorded (USGS, 2010e). The mean annual flow for the period of record is 941 cfs (USGS, 2010e).

A closer representation of the hydrology at the LLHR site, and the second nearest gaging station to the site, is USGS 08330000 Rio Grande at Albuquerque, NM. This gage has a much longer period of record than the gage at Bosque Farms, extending from March of 1942 to present. The flows are regulated by all the same upstream dams: Heron, El Vado, Abiquiu, Cochiti, Galisteo and Jemez Dams. It experiences one of the two agricultural diversions and the same municipal diversion. Based on the water years from 1974 (the year after Cochiti Dam began operations) to 2009, the maximum peak flow was 8,650 cfs (245 cms) on April 24, 1985 and the 10% exceedance flow is 3,360 cfs (95 cms) (USGS, 2010c).

Figure 2 shows the mountain ranges, major tributaries, dams, and stream gages of the Middle Rio Grande upstream of the LLHR project site. Figure 3 shows the monthly average daily flows retrieved from the USGS (2010a, 2010e) for the period of record at USGS Gage 08331160 Rio Grande near Bosque Farms, NM, for the water years from 1974 to 2009 at USGS 08330000 Rio Grande at Albuquerque, NM, and for the water years from 1971 to 2009 at USGS 08313000 Rio Grande at Otowi Bridge near San Ildefonso, NM. Higher values from December to February at USGS 08330000 Rio Grande at Albuquerque, NM compared to USGS 08313000 Rio Grande at Otowi Bridge near San Ildefonso, NM are due to releases from Cochiti Dam in preparation for high volumes of spring runoff.

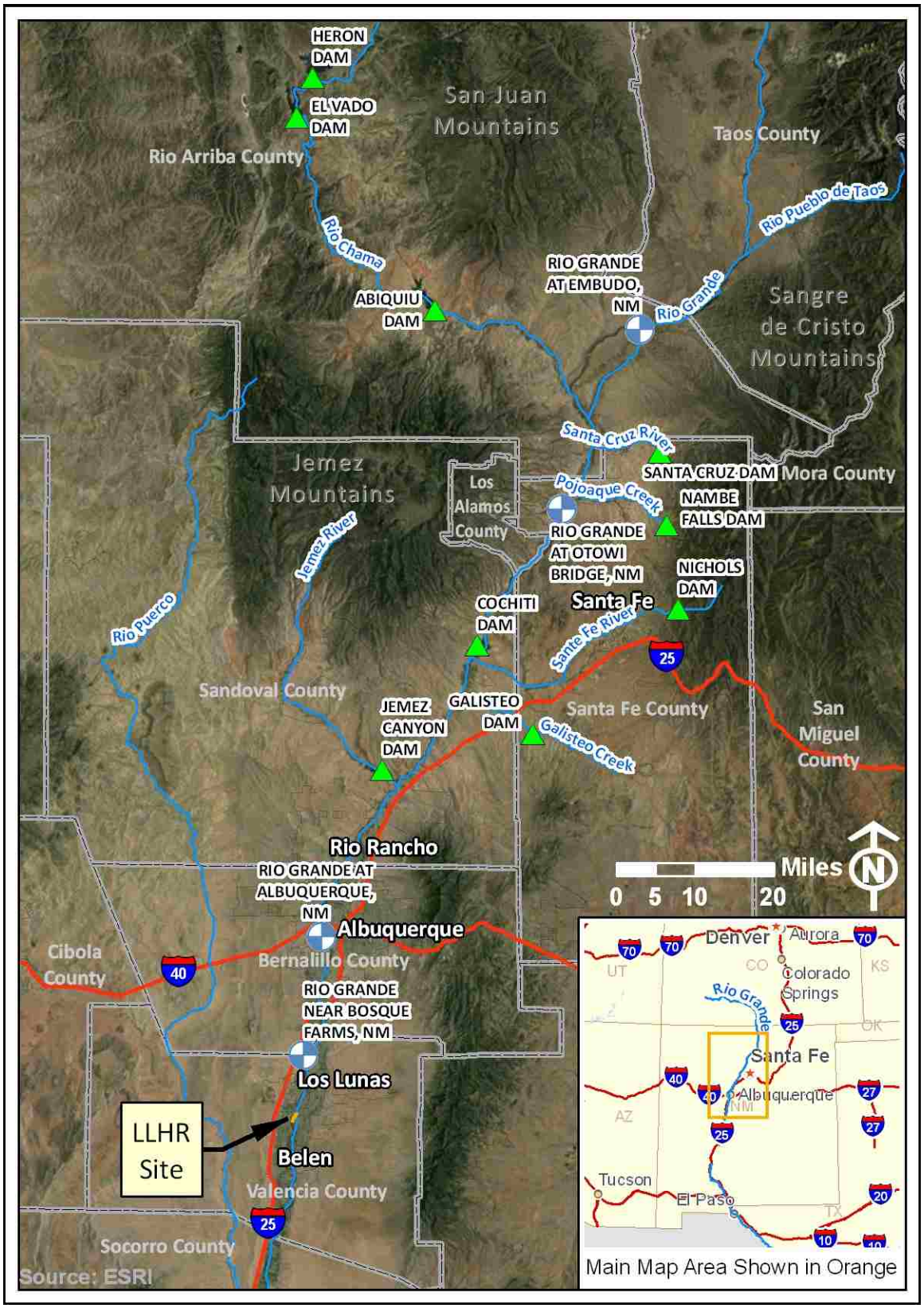

Figure 2: Map of Los Lunas Habitat Restoration site with dams and major stream gages

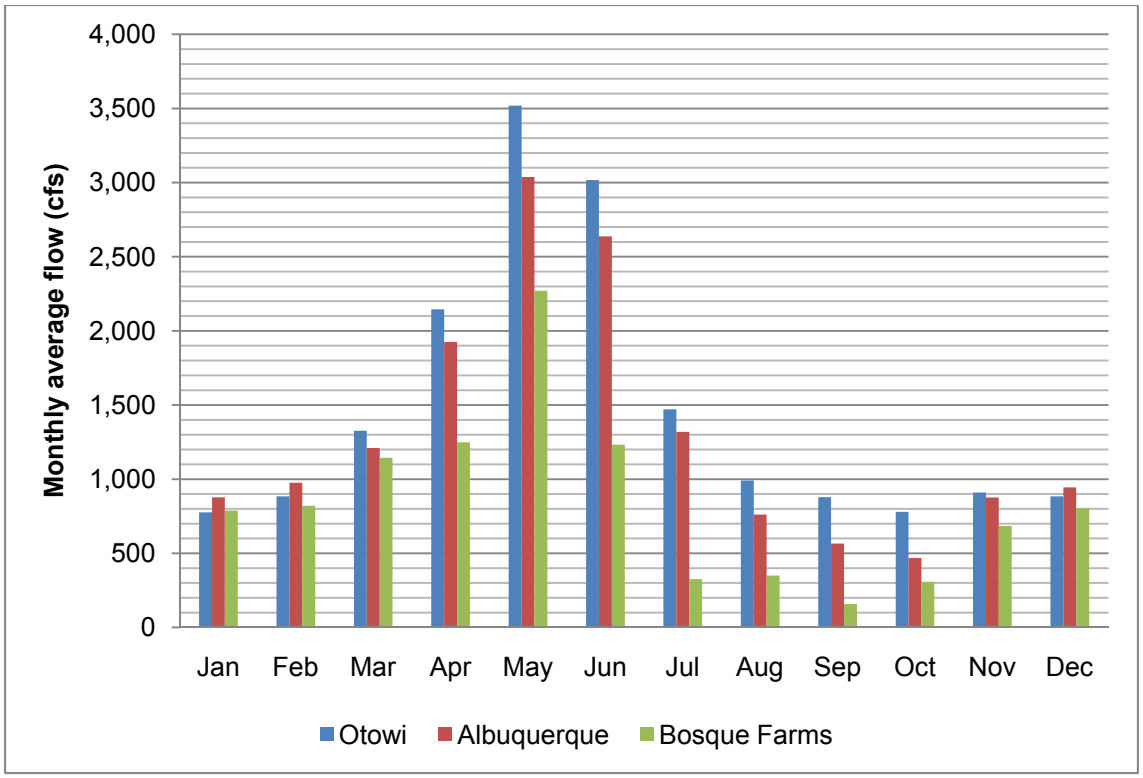

Figure 3: Monthly averaged daily flows at the USGS 08313000 Rio Grande at Otowi Bridge near San Ildefonso, NM, USGS Gage 08330000 Rio Grande at Albuquerque, NM, and USGS Gage 08331160 Rio Grande near Bosque Farms, NM

Hydraulics

Levees were constructed in the 1930s by the MRGCD from Belen to Los Lunas and hydraulic analysis by the USACE indicated that the levees provide protection against a 7,500 cfs flow corresponding to the 5% (20-year) storm event (FEMA, 2010). The New Mexico Interstate Stream Commission (NMISC) utilized the 2008 LiDAR data to complete a hydraulic model for "understanding and monitoring" of targeting specific instream sand bars and islands for mechanical lowering to promote more frequent inundation to increase habitat quality in the Rio Grande (A. Lundahl, personal communication, June 14, 2010). A study conducted by the USBR (Slaugh, 2003) was

undertaken to assess the water usage by the LLHR site, with the NMISC concerned that the as-built design was in fact inundating at lower flows than specified (Slaugh, 2003). This study addressed the amount of water in the LLHR under specific flow conditions but did not address habitat considerations in the LLHR. The report showed that the side channel invert was approximately 0.5 feet lower than the design, facilitating evaporation on almost 10 acres of open water at the 1,000 cfs flow rate, and the upstream side channel was closed off by raising the channel invert (Slaugh, 2003).

HEC-RAS

The U.S. Army Corps of Engineers Hydrologic Engineering Center (HEC) publishes and maintains River Analysis System (HEC-RAS) software which is free via its Website, http://hec.usace.army.mil. The HEC-RAS software has become accepted in many fields of hydraulic engineering including floodplain delineation (Cook & Merwade, 2009; Noman, Nelson, & Zundel, 2001; Omer, Nelson, & Zundel, 2003), one-dimensional hydraulic modeling (Casas, Benito, Thorndycraft, & Rico, 2006; Shatnawi & Goodall, 2010), flood propagation (Castellarin, Di Baldassarre, Bates, & Brath, 2009) and many others applications such as ice jam breaks, dam removal, water quality and sediment mobility.

The Manning Equation. The HEC-RAS model relies on the equation developed by Robert Manning in 1885 while working as the chief engineer of the Irish Office of Public Works in Dublin. It was developed using the best known empirical formulas at the time, developed by Du Buat in 1786, Eyelwein in 1814, Weisbach in 1845, St. Venant in 1851, Neville in 1860, Darcy and Bazin in 1865, and Ganguillet and Kutter in 1869 (Khoury, 2005). The equation is an empirical solution for velocity in open channels

based on measurable parameters and channel-specific coefficients, but its fundamentals rest on the pure mathematical equations by Newton, Leibniz, Bernoulli and Euler (Sturm, 2010). Manning developed a best-fit equation for the velocity calculated by each of the formulas for a given slope and varying hydraulic radius (Khoury, 2005). The formula, $V = CR^{2/3}S^{1/2}$, was presented in 1889 to the Institution of Civil Engineers in Ireland (Khoury, 2005) more than 10 years after Philippe Gauckler presented the same formula in 1868 (Sturm, 2010). The textbook "Handbook of Hydraulics" by Horace Williams King, which became popular after its release in 1918, attributed the equation to Manning and presented the coefficient C as 1/n, leading to the widespread use of the Manning equation in its current form, $V = (1/n)R^{2/3}S^{1/2}$ (Khoury, 2005). The formula calculates velocity (V) as a function of hydraulic radius (R), energy slope (S) and a channel friction coefficient (n) which has since come to be known as the Manning's *n* value. A slight variation, $V = (1.486/n)R^{2/3}S^{1/2}$, uses U.S. customary units. The hydraulic radius is defined for open channels as the ratio of the cross sectional water area normal to flow to the wetted perimeter of the channel, having units of length (Chow, 1959). The energy slope is the difference in total head from one location to another, in units of length, and being the sum of elevation, pressure head (depth), and velocity head (Chow, 1959).

HEC-RAS software. The software documentation (Brunner, 2010a) includes a full description of the fundamental assumptions and the types of calculations or simulations available. It is designed for one-dimensional analysis of any manner of channel designs and flow regimes including natural channels with unsteady flows (Brunner, 2010a). The fundamental mathematics of steady flow modeling is based on the one-dimensional energy and momentum equations (Brunner, 2010a). The momentum

equation is applied in the HEC-RAS model only to the specific situations of hydraulic jumps, low flow associated with structures, and stream junctions (Brunner, 2010a). These situations are not encountered in this study therefore discussion of the momentum equation is not included.

The energy equation assumes the conservation of energy of an incompressible fluid with some losses and solves by equating the upstream total energy to the downstream total energy plus losses. Total energy is comprised of potential energy and kinetic energy. Most hydraulic systems are sloped and the potential energy is a sum of the water surface depth above the channel bed and the bed elevation above an arbitrary datum. This method allows simple extraction of the water depth from the equation as the energy slope is generally an assumed input value. The energy equation for channels of small slopes and gradually varied flow (Chow, 1959) is:

$$z_1 + d_1 + \alpha_1 \frac{V_1^2}{2g} = z_2 + d_2 + \alpha_2 \frac{V_2^2}{2g} + h_e \qquad \text{Equation 1}$$

where:

z_1, z_2 = elevation of the channel bottom above a datum

d_1, d_2 = depth of water at cross sections

$\alpha 1$, $\alpha 2$ = energy coefficients

V_1, V_2 = average velocities (total discharge divided by total flow area)

g = gravitational acceleration constant

h_e = loss of energy head

The energy head loss between cross sections in HEC-RAS (Brunner, 2010a) is:

$$h_e = L\bar{S}_f + C\left|\frac{a_2 V_2^2}{2g} - \frac{a_1 V_1^2}{2g}\right| \quad \text{Equation 2}$$

where:

L = discharge-weighted reach length

$\bar{S}_f$ = representative friction slope between cross sections

C = expansion or contraction loss coefficient

The discharge-weighted reach length, L, (Brunner, 2010a) is:

$$L = \frac{L_{lob}\bar{Q}_{lob} + L_{ch}\bar{Q}_{ch} + L_{rob}\bar{Q}_{rob}}{\bar{Q}_{lob} + \bar{Q}_{ch} + \bar{Q}_{rob}} \quad \text{Equation 3}$$

where:

L_{lob}, L_{ch}, L_{rob} = cross section reach lengths specified for flow in the left overbank, main channel, and right overbank, respectively

$\bar{Q}_{lob}, \bar{Q}_{ch}, \bar{Q}_{rob}$ = average of the flows for the left overbank, main channel, and right overbank, respectively

Merwade (2009) and Brunner (2010a) identified that to solve for steady, gradually varied flow, the equations for conservation of mass and energy in addition to Manning's equation can be used to compute an area-averaged water surface elevation given upstream and downstream boundary conditions. This process is done by subdividing the conveyance for each cross section. Each cross section is subdivided into the left and right overbanks and the main channel, typical locations where Manning's *n* values differ, and

conveyance in each subdivision is solved independently. The three computed conveyance values are summed to determine the overall conveyance of the cross section. Discharge is calculated using the Manning's equation for each subdivision and is then divided by the area of the subdivision to obtain velocity. The following two equations together comprise Manning's equation:

$$Q = KS_f^{1/2} \qquad \text{Equation 4}$$

$$K = \frac{1.486}{n} AR^{2/3} \qquad \text{Equation 5}$$

where:

Q = discharge

K = conveyance

S_f = friction slope between cross sections

n = Manning's roughness coefficient

A = flow area

R = hydraulic radius

The equations outlined above are too few to completely define the water surface elevation for each cross section. The above presentation covers only the steady gradually varied flow regime although the HEC-RAS software can solve unsteady flow regimes. Sturm (2010) identified HEC-RAS as using the secant method for solution and in the case of natural channels as using the standard step method. Brunner (2010a), Castellarin et al. (2009), Di Baldassarre and Montanari (2009), and Horritt and Bates (2002) identified the

use of the De Saint Venant equations, the finite difference method and the Preissmann four-point implicit method to solve for unsteady flow models.

Hydraulic parameters

The hydrology of the LLHR is determined with gage data and engineering specifications of the project, which are both straightforward. Other hydraulic parameters used in the HEC-RAS model are reach slope, hydraulic roughness, boundary conditions and flow regime. The reach slope is determined with the terrain model in ArcMap. Hydraulic roughness parameters are determined from published values of similar channels or measured in the field. Boundary conditions in HEC-RAS are set at the farthest upstream and downstream cross sections for each flow profile and can be in reference to either a known water surface elevation, critical depth, normal depth (including the slope), or rating curve (defined as a table of stage-flow pairs) (Brunner, 2010b). Although each flow profile requires boundary conditions, the software allows duplication of boundary conditions for all flow profiles. The flow regime is set to subcritical, supercritical or mixed before simulation.

Hydraulic roughness. The hydraulic roughness of a stream is spatially varied with substrate, vegetation cover, channel meander and other features which act as an impediment to flow. Hydraulic roughness is characterized in many hydraulic models, including HEC-RAS, with the Manning's *n* value. The spatial heterogeneity of Manning's *n* values is represented in ArcMap and translated to the HEC-RAS hydraulic model with HEC-GeoRAS.

Chow (1959) provides reference tables for Manning's *n* values with natural channels normally between 0.030 and 0.100, although those composed primarily of sand

with some gravel and flowing straight and cleanly can range from 0.025 to 0.040 with normal values of 0.030 to 0.035. Chow (1959) also provides floodplain Manning' n values ranging from 0.025 to 0.160 although those composed of medium to dense brush in summer range from 0.07 to 0.160 with normal values of 0.100. The substrate at the LLHR site reach has been shown by Slaugh (2003) to be composed primarily of sand with some gravel and numerous islands in the channel. The San Marcial reach was calibrated to a Manning's *n* value of 0.025 and is very similar in channel substrate (Slaugh, 2003). A sensitivity analysis of Manning's *n* values versus flow produced small differences in the water surface elevation (0.25 ft) at flow rates of 500 and 1,000 cfs (Slaugh, 2003). Isaacson (2009) based Manning's *n* values on modeling studies completed by the USACE and measurements by Nordin (1964), assigning 0.02 for the river channel, 0.05 for islands and 0.08 for the riparian corridor within the Albuquerque reach of the Rio Grande. A direct study of the measurements at the San Acacia gage showed values of Manning's *n* values in agreement with a mean of 0.026 (Leon, Julien, & Baird, 2009). The same study also examined sediment transport above Elephant Butte Reservoir and calibrated Manning's *n* values to 0.024 (Leon et al., 2009). San Acacia, San Marcial and Elephant Butte Reservoir are approximately 40, 80, and 125 river miles south of the LLHR site, respectively.

Vegetation affects hydraulic roughness due to spatial variation in vegetation type (Chow, 1959), temporal variation as vegetation changes over the seasons (De Doncker, Troch, Verhoeven, Bal, Meire, & Quintelier, 2009; Di Baldassarre & Montanari, 2009), and variation relative to height of vegetation (Stephan & Gutknecht, 2002; Cobby, Mason, Horritt, & Bates, 2002; Wang, P., Wang, C., & Zhu, 2010). Because the study

proposed here is centered on habitat analysis, hydraulic roughness due to seasonal changes in vegetation is not necessary. However, spatial variation of hydraulic roughness due to vegetation is important in habitat analysis and especially so in relation to sand bars and islands.

The variability of hydraulic roughness at the LLHR site is due to vegetation in the overbanks and low velocity side channels. The vegetation at the LLHR site is composed mainly of forbs (43.6% cover), grasses (14.5% cover), and shrubs (18.8% cover) (Siegle & Reed, 2007). Of the shrub classes found, cottonwood saplings are most abundant followed by almost equal amounts of saltcedar and coyote willow (Siegle & Reed, 2007). Although cottonwoods become quite large, 20 – 40 m in height and trunks often 1 m or more in diameter (National Resources Conservation Service [NRCS], 2010a), the fire in 2000 cleared all the vegetation and currently the cottonwood specimens are saplings no more than 10 years of age. Willow and saltcedar trunks are generally very thin but grow in very dense stands and the shrubs can reach heights of 15 feet (NRCS, 2010b, 2010c).

Ineffective flow area features are used in HEC-RAS to simulate the flow across densely vegetated sand bars and islands. These features identify areas of the cross section where flow is stagnant or nearly so (Ackerman, 2009; Brunner, 2010a). The flow in this type of area is zero until the water surface reaches a specified height. The ineffective flow areas are modeled to contain water volume, which has effects on calculations of the cross section storage, wetted perimeter and water surface profile (Brunner, 2010a).

Hsieh and Bolton (2007) found that although channels were sparsely vegetated, the velocity of flow in the channel decreased dramatically. The study was a

mathematical evaluation of laminar flows in response to differing heights of vegetation. Depths and flows were normalized to the values computed without vegetation. The authors show vegetation having a height as small as one-quarter of the water depth reduced channel velocity by half (Hsieh & Bolton, 2007). A vegetation porosity of 0.95 slowed velocity to zero until it was completely submerged to a depth almost half of the vegetation height (Hsieh & Bolton, 2007).

Boundary conditions. Boundary conditions in the HEC-RAS model require either a known water surface elevation or rating curve, otherwise a determination that the flow is at a normal or critical depth (Brunner, 2010b). Without a known water surface elevation or surveyed datum for the local USGS stream gages to utilize a rating curve directly, the boundary condition is set to normal flow depth and slopes are required. When using a supercritical flow regime, only the critical depth boundary condition at the upstream end of the reach is required, but a subcritical flow regime requires the energy slope at the downstream end which can be approximated using the bed slope (Brunner, 2010a). Assuming gradually varied flow, which is consistent with hydraulic modeling in HEC-RAS (Brunner, 2010a), and flow in a prismatic channel, the normal depth is found using Manning's equation and the critical depth is found by setting the Froude number equal to unity (Sturm, 2010). These values are then compared with the stage-discharge rating curve for the local USGS stream gage to determine whether normal or critical flow is more likely.

The ArcMap 3D Analyst tools are useful to determine the channel bed slope. Based on a DEM, features digitized in two-dimensions are converted to three-dimensional features using the "Convert Features to 3D" tool (ESRI, 2009). The stream

centerline feature is converted to a three-dimensional feature and its profile data are exported as station-elevation pairs into Microsoft™ Excel for analysis. A study by the USBR determined the slope in the reach below the San Acacia Diversion dam to vary from 60 to 80 cm/km (0.00060 to 0.00080 ft/ft) (Leon et al., 2009).

Inundation modeling

The results from HEC-RAS are taken into ArcMap via HEC-GeoRAS to delineate floodplains and map water surface extents, depths and average velocities. In ArcMap, floodplains can be evaluated using topography, aerial imagery and any previous floodplain mapping which has been digitized.

Horritt and Bates (2002) used two separate flood events on the same river and remotely sensed maps of flood extents to evaluate the effectiveness of a one-dimensional model (HEC-RAS) and a two-dimensional model (TELEMAC-2D). The authors found that both can be calibrated with discharge or area of inundation to yield good predictions of floodplain extents.

Cook and Merwade (2009) compared the hydraulic model FESWMS to HEC-RAS and found that HEC-RAS over-predicted the floodplain and showed more variability in the inundation area. Furthermore, the estimated inundation in both models decreased with increasing horizontal resolution, vertical accuracy and the inclusion of bathymetry in the topography (Cook & Merwade, 2009).

Critical shear stress

As the depth and velocity of the water over the sand-bed stream increase, the shear stress increases to a point at which the sand begins to move. The mobility of the

sediment indicates the balance between erosion and deposition, with a preference for one over the other leading to long term geomorphic changes. Changes to the geomorphic features subject to degradation by the river flow, such as the mid-channel and overbank sand bars, directly influence the hydraulics and therefore the habitat suitability of the site. The critical shear stress at the time of the initiation of motion and can be described in terms of an empirical relationship between two dimensionless parameters, the Shields parameter, τ_*, and the grain Reynolds number, R_* (Cao, Pender, & Meng, 2006; Ho, Coonrod, Gill, & Mefford, 2010; Marsh, Western, & Grayson, 2004; McLean, Wolfe, & Nelson, 1999; Sarmiento & Falcon, 2006; Wiberg & Smith, 1987; Sturm, 2010).

The grain Reynolds number is the product of critical shear velocity and grain diameter divided by kinematic viscosity (Sturm, 2010). Cao et al. (2006) and Sturm (2010) present the grain Reynolds number without the critical shear velocity and in terms of median grain diameter, i.e. diameter at which 50% of the sample is heavier, submerged specific weight of the sediment and kinematic viscosity:

$$R_* = \frac{d_{50}\sqrt{sgd_{50}}}{\upsilon} \qquad \text{Equation 6}$$

where:

R_* = grain Reynolds number

d_{50} = median grain diameter

s = submerged specific weight of the grain

g = gravitational acceleration constant

υ = kinematic viscosity of the fluid

Cao, et al. (2006) and Sturm (2010) define submerged specific weight as:

$$s = \frac{\rho_s}{\rho} - 1 = \frac{\gamma_s}{\gamma} - 1 \qquad \text{Equation 7}$$

where:

ρ_s = density of the grain

ρ = density of the fluid

γ_s = specific weight of the grain

γ = specific weight of the fluid

The Shields parameter is defined as the shear stress divided by the product of submerged specific weight of the grain and grain diameter at critical conditions (Sturm, 2010). The grain diameter term is taken as the median grain diameter, d_{50}, (Sturm, 2010).

$$\tau_* = \frac{\tau_c}{(\gamma_s - \gamma) d_{50}} \qquad \text{Equation 8}$$

where:

τ_* = Shields parameter

τ_c = critical shear stress

The Shields parameter can be directly determined using a third parameter, the dimensionless grain diameter, d_*, (Sturm, 2010) as:

$$d_* = \left[\frac{(\gamma_s/\gamma - 1)\mathrm{g}\mathrm{d}_{50}^3}{\upsilon^2}\right]^{1/3} \quad \text{Equation 9}$$

where:

d_* = dimensionless grain diameter

Equation 9 can be related to the grain Reynolds number and Shields parameter (Sturm, 2010) using:

$$d_* = \left[\frac{R_*^2}{\tau_*}\right]^{1/3} \quad \text{Equation 10}$$

Equations 6 and 9 are used to determine the grain Reynolds number and the dimensionless grain diameter, respectively. Equation 10 is then used to determine the Shields parameter for use in Equation 8 to solve for the critical shear stress.

Cao et al. defined a dimensionless critical Shields parameter in terms of the critical bed shear stress and "nondimensionalized" this using fluid and sediment properties at the point when sediment is nearing mobility (Cao et al., 2006, p. 1097). The dimensionless critical Shields parameter, θ_c, (Cao et al., 2006; Sturm, 2010) is:

$$\theta_c = \frac{\tau_c}{(\rho_s - \rho)g d_{50}} = \frac{\tau_c}{(\gamma_s - \gamma)d_{50}} \quad \text{Equation 11}$$

where:

θ_c = critical Shields parameter

Cao et al. (2006) utilized the critical Shields parameter, θ_c, and the shear Reynolds number to derive a trio of analytical relationships between the critical Shields parameter and grain Reynolds number:

$$\theta_c = 0.141 R_*^{-0.2306} \qquad R_* <\approx 6.61 \qquad \text{Equation 12}$$

$$\theta_c = \frac{\left[1+(0.0223R_*)^{2.8358}\right]^{0.3542}}{3.0946 R_*^{0.6769}} \qquad R_* \in (6.61, 282.84) \qquad \text{Equation 13}$$

$$\theta_c = \frac{\tau_c}{(\rho_s - \rho) g d_{50}} \qquad R_* > \approx 282.84 \qquad \text{Equation 14}$$

These relationships are used to estimate the stability of the sand bed channel at the LLHR project site in the geospatial analysis using results from the hydraulic modeling.

LiDAR-based hydraulic modeling

Modeling of stream hydraulics is driven by data resolution. It has been shown that topography is the limiting factor in the quality of the hydraulic model in representing flows in an open channel (Casas, Benito, Thorndycraft, & Rico, 2006; Bates, Marks, & Horritt, 2003; French, 2003; Marks & Bates, 2000; Merwade, Olivera, Arabi, & Edleman, 2008; Schumann, Matgen, Cutler, Black, Hoffman, & Pfister, 2008; Shatnawi & Goodall, 2010). Additionally, hydraulic modeling is quite sensitive to the typically low relief of a river floodplain and small differences can have large consequences in floodplain delineation (Casas et al., 2006). Traditional surveys have become more expensive and are "constrained by the limited spatial resolution" (Bates et al., 2003, p.

537) in comparison to LiDAR surveys which can cover up to 90 km² per hour with vertical resolution of ±10 – 15 cm and can be completed day or night and in most weather conditions (French, 2003; Marks and Bates, 2000). The comparison between models of differing resolutions has shown that those with coarse resolution poorly estimate the flood inundation potential (Casas et al., 2006; Merwade et al., 2008; Shatnawi & Goodall, 2010). In some cases, the floodplains are overestimated (Casas et al., 2006) leading to unreliable maps and costly flood insurance. In other cases, the floodplains are underestimated (Marks & Bates, 2000) potentially leading to catastrophic and deadly consequences.

Schumann et al. (2008) used measured flood stage values to compare hydraulic modeling results from three terrains: LiDAR terrain data with horizontal and vertical accuracies of 2 m and 15 cm, respectively; a 50 m DEM derived from contour maps; and 3 arc-second Shuttle Radar Topography mission (SRTM) data. The authors found the LiDAR data performed best; stages were modeled to within 0.35 m (1.15 ft) of measured values. The 50 m DEM and SRTM data were found to predict flood stages within 0.7 m (2.30 ft) and 1.07 m (3.51 ft), respectively. The authors found SRTM data, in the hands of experienced modelers and engineers, to be a viable candidate to determine the potential of flood inundation in many areas of the world where LiDAR surveys and contour maps are not feasible or available (Schumann et al., 2008).

At the LLHR site, terrain data were collected using LiDAR equipment in March of 2008. A review of the data indicates that over the course of three days there was overlap of data collection. This overlap increases the data resolution of features which are time-insensitive in the short term, such as vegetation and ground surface.

Overlapping LiDAR collections of time-sensitive features such as water in a flowing river introduces conflict; however, data are filtered out by time to preserve consistency. The calibration of the LiDAR data includes hydraulic modeling of the terrain adjacent to the gage yielding a correlation of LiDAR data to measured river stage, or leads to a decision to remove LiDAR classified as water. This geospatial processing is completed using the GIS software package ArcMap from ESRI™.

Ecology

The Endangered Species Act

The Endangered Species Act, or ESA, has become a powerful and contentious issue for many communities and organizations in the United States. The foundations were first laid with the passing of the Endangered Species Preservation Act in 1966 which authorized the U.S. Fish and Wildlife Service (USFWS) to purchase and maintain land for the purpose of protecting habitat within the National Wildlife Refuge System (Stanford Environmental Law Society, 2000). The first list with 78 endangered species was issued early the following year by the late Secretary of the Interior, Stewart Udall (1920-2010), who stated that "the following listed native fish and wildlife are threatened with extinction," and included 14 mammals, 36 birds, 6 reptiles and amphibians, and 22 fish (Udall, 1967, p. 4001). Included in this list were grizzly bears, California condors, bald eagles, alligators, manatees, two species of wolves, and five species of trout (Udall, 1967). The law was amended with the passing of the Endangered Species Conservation Act in 1969 which expanded protection to invertebrate species and provided listed

species global protection by excluding them from being traded into the United States from abroad. The passing of the ESA in 1973 required that habitat be identified as critical to the recovery of listed species, including physical or biological features which may or may not have the listed species currently in residence (USFWS, 2009). As of February 2010, the USFWS had listed 379 vertebrate animals, 198 invertebrates, 718 flowering plants, and 31 non-flowering plants (such as conifers, ferns, lichens, and algae) for a total of 1,215 animals and 752 plants (USFWS, 2010b). More importantly, between 1972 and 2005 only 22 listed species have gone extinct and these are now considered to have been at populations so low at the time of listing that recovery was implausible (Goble, Scott, & Davis, 2005).

Federal agencies are required to coordinate with the USFWS in order to promote the recovery of listed species. To do this, agencies submit Biological Assessments which are used by the USFWS to produce a Biological Opinion (BO), the most recent for the MRG area is dated June 2001. Agencies are required to comply with the BO issued by the USFWS in order that the agency's authorized action does not negatively impact the listed species (USFWS, 2009). Part of the coordination with the BO is the identification of a currently occupied or potential critical habitat which cannot be negatively impacted by the agency's actions. An economic analysis has the ability to negate the designation as critical habitat (USFWS, 2009). The critical habitat for the minnow is defined as a 300 foot width along 157 stream miles of the Rio Grande from below Cochiti Dam to Socorro County and another 300 foot width along 55 miles of the Jemez River from the Jemez Canyon Dam to the Pueblo of Santa Ana for a total of 212 miles in the Rio Grande basin (USFWS, 2003). Although the critical habitat for the minnow ceases in Socorro County,

the recovery plan for the species extends to Elephant Butte Reservoir (USFWS, 2010a). The critical habitat of the flycatcher in New Mexico is defined as Grant, Hidalgo, Mora, Rio Arriba, Socorro, Taos, and Valencia counties (USFWS, 2005). Several of these counties are in the Rio Grande basin or are directly on the river, as shown in Figure 1. The LLHR site is located in Valencia County.

The flycatcher is a Neotropical migratory bird which nests in densely vegetated riparian areas and grow to approximately 5.75 in (15 cm) long and 0.42 oz (12 g) in weight (USFWS, 2002). The minnow is approximately 3.5 in (89 mm), males and females show little difference in appearance, and the species as a whole has been incorrectly classified several times since 1856 (USFWS, 2010a). The minnow and flycatcher are depicted in Figure 4 and Figure 5, respectively.

Figure 4: Rio Grande silvery minnow (Hybognathus amarus)

Figure 5: Southwestern willow flycatcher (*Empidonax traillii extimus*)

Recent restoration efforts

The burned LLHR site provided a unique opportunity to environmental managers to interrupt the proliferation of invasive and non-natives species, establish native habitat, and provide critical habitat of endangered species. The site burned in 2000 and the restoration construction project began in 2002 with habitat monitoring commitments planned until 2017 (Siegle & Reed, 2007). The goals were to engineer the project surface to inundate at flows of 2,500 cfs and to inundate a series of inlets along the banks for flows less than 2,500 cfs (Siegle & Reed, 2007). Inundation not only allows for minnow habitat but "the increased inundation frequency would begin the process of post-fire regeneration of high-value existing and revegetated terrestrial habitats in portions within and adjacent to the restoration area to support the recovery of the SWFL [southwestern willow flycatcher]" (Siegle & Reed, 2007, p. 1). Variable depth channels were constructed to aid in minnow egg retention and rearing habitat. By the end of the construction phase, 1,400 jetty jacks were removed and approximately 40 acres of shallow and low velocity aquatic habitat was created with restored native vegetation

(Siegle & Reed, 2007). The LLHR site restoration project features are shown in Figure 6. The removal of the channel-stabilizing jetty jacks allows the river to develop a more natural meander within the confines of the levee system. The root wad berm is a linear earthen mound built up around root wads, a mass comprising of the trunk, roots, soil, and rock that remains intact when the tree is uprooted. The root wad berm controls the overall inundated area to conserve water and focuses the inundation to the engineered features.

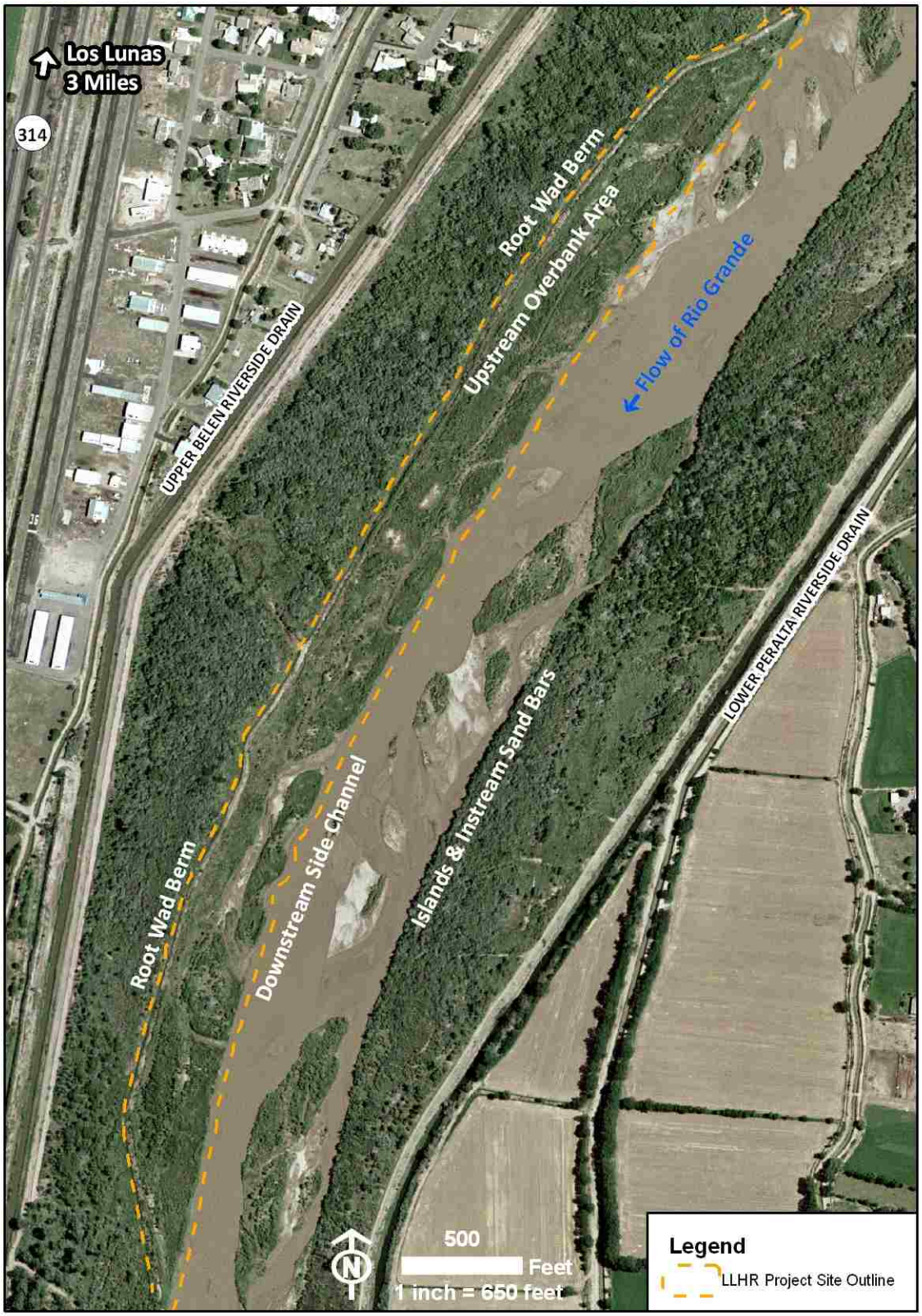

Figure 6: Los Lunas Habitat Restoration project area and features

Until the study presented here, habitat analysis derived from hydraulic modeling has not been initiated following the restoration activities. Hydraulic analysis is crucial so that planners can determine if and how the site will continue to provide suitable habitat to both endangered and native species in the long term. Analysis of both the transverse channels and instream sand bars in relation to the inundation regime can show stability of these critical habitat features while identifying other features which may require maintenance. For example, deposition of sediment within the low velocity side channels decreases the utility of these features if hydraulic connectivity with the river becomes compromised. Loss of connectivity can lead to high minnow mortality as inundation recedes. In addition, roughness of the overbank areas has likely been increased by the establishment of vegetation, formation and vegetation of sand bars, and a transition from saltcedar to willow and cottonwood species. This increase in overbank roughness will decrease water velocity and further increase sediment deposition.

Habitat studies

Regulated flow regimes have been shown to diminish habitat quality for a number of species including the minnow, the flycatcher, willows, and cottonwoods which all have life stages dependent upon increased peak flows not typical in regulated systems (Hatch & Gonzales, 2009; Rood & Mahoney, 1990; Poff, Allan, Bain, Karr, Prestegaard, Richter, Sparks, & Stromberg, 1997; Shafroth, Stromberg, & Patten, 2002; USFWS, 2002; Dudley & Platania, 2007). Flow regulation, channelization and habitat fragmentation have decreased the habitat suitability for the minnow, especially within the early stages of life (Hatch & Gonzales, 2009; Dudley & Platania, 2007). Minnow spawning is coincident with high spring flows when floodplains are inundated to form

shallow pools wherein large numbers of eggs and larvae are retained and shielded from the higher flow rates in the main channel (Hatch & Gonzales, 2009; Dudley & Platania, 1997). Among other effects of flow regulation was loss of habitat for numerous species and the proliferation of invasive and non-native species such as saltcedar (Glenn & Nagler, 2005). Backwater channels with shallow depths and low velocities aid in minnow egg retention and rearing habitat (USFWS, 2010a). Increased duration of inundation discourages invasive species such as saltcedar (Lesica & Miles, 2004), but does not hinder establishment and survival of cottonwood and willow (Shafroth el al., 2002).

Habitat characteristics have been studied for the minnow. Dudley and Platania (1997) collected mesohabitat availability and use for the minnow at two locations along the Rio Grande in New Mexico, near the towns of Rio Rancho (upstream of the LLHR) and Socorro (downstream of the LLHR). The authors found preference of similar depth and velocity mesohabitats although differences in substrate were noted. The distribution of water depth preference for both sites was bimodal with peaks at the collection ranges of 11 – 20 cm (4.3 – 7.9 in) and 31 – 40 cm (12.2 – 15.7 in) with little or no preference shown for depths less than 10 cm or greater than 50 cm. The preference for water velocity was clearer with 87% of individuals collected at both sites (83% at Socorro) in velocities less than 10 cm/s (0.33 ft/s) (Dudley & Platania, 1997). There was no difference in preference of mesohabitat by the size of individual despite "considerable differences" in habitat availability (Dudley & Platania, 1997, p. 57). The minnow preferred the silt substrate at the Socorro location "more than would be predicted from its

availability" (Dudley & Platania, 1997, p. 57). The substrate conditions at Socorro most resemble those at the LLHR site.

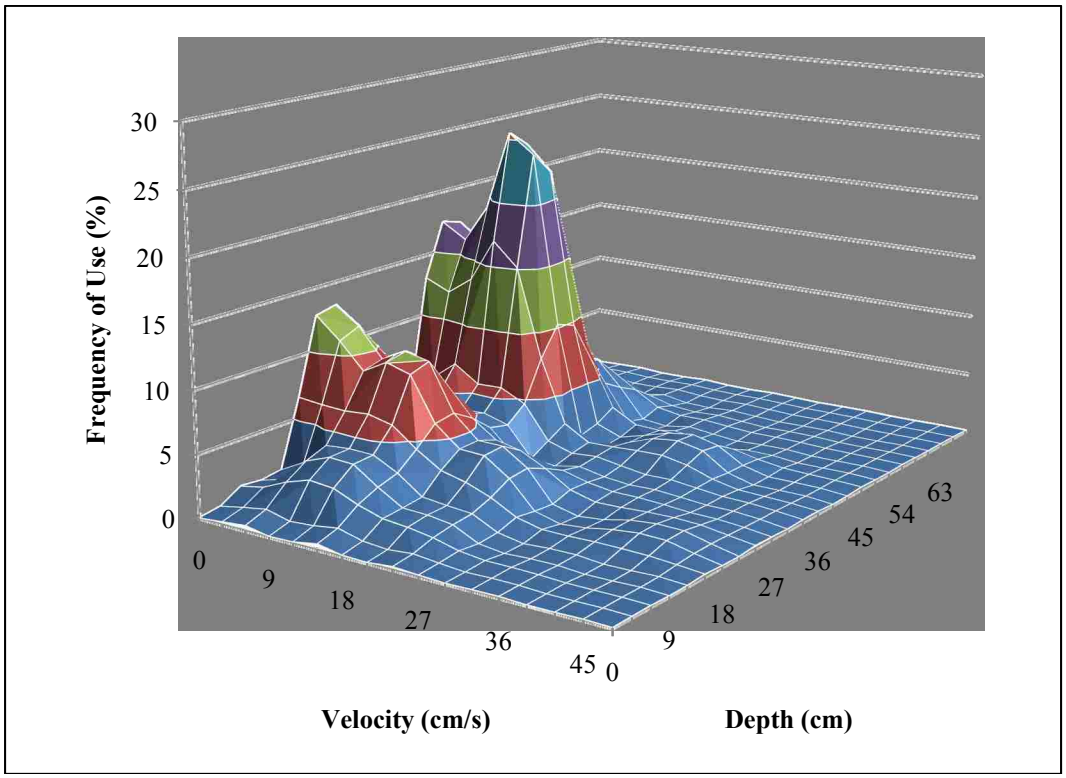

Figure 7: Frequency of habitat use of the Rio Grande silvery minnow (*Hybognathus amarus*) by depth and velocity

Note. Interval is 3 cm on depth scale and 3 cm/s on velocity scale. Adapted from R. K. Dudley and S. P. Platania, 1997, *Habitat use of the Rio Grande silvery minnow.*

Stream hydraulics have been used by ecologists to predict and statistically describe habitat suitability and preferences by quantitative analyses (Jowett 2003; Lobb & Orth 1991; Statzner, Gore & Resh, 1988), and more recently with geospatial mapping (Jowett, 2003; Le Coarer, 2007). These data and studies of fish preferences for habitat hydraulic characteristics are analyzed in a GIS environment to map predictions of habitat use and perform statistical calculations to determine size and extent of available habitat.

The subset of an overall habitat delineated by preferred depth and velocity is referred to here as mesohabitat; in the literature this term can refer to any combination of delineated stream habitat characteristics as defined by the author. Habitat characteristics have been studied for the minnow (Dudley & Platania, 1997, 2007), but hydraulic modeling for the prediction of fish habitat preferences using geospatial analysis has not been performed.

The hydraulic characteristics of the preferred mesohabitat for the Barbel (*Barbus barbus*) and the Blageon (*Leuciscus souffia*) in the Durance River of France are described by Le Coarer (2007) using the method of depth-velocity indices and introducing the term *hydraulic signatures* to describe the spatial extent and availability of mesohabitat. Field measurements of the depth and velocity profiles across numerous cross sections were used to compute volumes of each depth-velocity class. The percentage of each depth-velocity volume relative to the total volume of the reach is defined by the author as the hydraulic signature (Le Coarer, 2007). In the same manner of a volumetric hydraulic signature, a preference index is obtained with measuring depth and velocity when sampling fish distribution: for each fish obtained via electro-fishing, measurements of depth and velocity are recorded and the totals are summed and normalized by depth-velocity classes. Le Coarer (2007) then shows mapping of the spatial distribution of habitat preference in terms of availability for the two fish species.

According to the endangered species recovery plan for the flycatcher, its habitat is concentrated in dense riparian areas with vegetation from ground level into a canopy nearly 100 ft off the ground (USFWS, 2002). Breeding habitat includes sites with dense vegetative cover within 3 – 4 m (10 – 13 ft) of the ground (USFWS, 2002). Nesting habitat occurs over a wide range, 2 – 30 m (6 – 98 ft), in densely vegetated thickets

(USFWS, 2002). This range would include the canopy of willow and cottonwood species, both as saplings and mature vegetation. The average canopy height of nesting habitat is 3 – 7 m (10 – 23 ft) (USFWS, 2002), which represents mature willows or cottonwood saplings. The flycatcher's preference of native over exotic vegetation is shown by the USFWS (2002) using 950 known territories of which 468 are located in habitat types with over 90% native vegetation, 392 are in half-native, half-exotic vegetation, and only 90 are located in habitat with over 90% exotic vegetation types. The same study (USFWS, 2002) shows a preference of nesting sites in native vegetation with 1,111 (55%) sites located in various native species and 768 (38%) located in saltcedar stands; if the sites composed of 90% willow and 10% exotic species are included the preference for native vegetation rises to 1,214 sites (60%). The percent of successful nests (fledging at least one flycatcher) in New Mexico is 90% for all sites dominated by native vegetation (USFWS, 2002).

Table 1: Habitat preferences for the Southwestern willow flycatcher (*Empidonax traillii extimus)*

Habitat Type	Number of Territories	Number of Nests	Number of Successful Nests
Native	468	1,111	414
Mixed	392	103	35
Exotic	90	768	49

Note. Native habitats are those with less than 10% cover of exotic species, Mixed habitats have more than 10% exotic, and Exotic habitats have more than 90% exotic. Adapted from the U.S. Department of the Interior, Fish and Wildlife Service, 2002, *Final recovery plan for the Southwestern willow flycatcher*.

Vegetation monitoring has shown that the LLHR site is performing well in excluding nonnative and invasive vegetation species from dominating the native vegetation (Siegle & Reed, 2007). In 2003, 63.5% of the LLHR site was bare soil with forbs and grasses comprising the remainder (Siegle & Reed, 2007). By 2006, 17.7% was native shrubs (including cottonwood saplings) with only 6.8% composed of saltcedar and Russian olive (Siegle & Reed, 2007).

Habitat modeling provides information on the utilization of a habitat by one or more species. Restoration projects are often left without plans for long-term monitoring once the habitat is established (Bash & Ryan, 2002; Kondolf & Micheli, 1995; Shields, Cooper, Knight & Moore, 2003), although some projects most certainly have very complete monitoring projects (Densmore & Karle, 2009; Downs & Kondolf, 2002; Shields et al., 2003). When restoration projects are being designed, the costs associated with stream restoration are weighed against the benefits the future habitat provides to targeted species. Hydraulic and ecological modeling provides justification for those projects which may otherwise not be undertaken due to insufficient information on the future performance of restored habitat. Those projects with sufficient funding for long-term monitoring are supplemented with hydraulic and ecological modeling. The performance and sustainability of completed stream restoration projects is quantified with hydraulic and ecological modeling.

Methods

Terrain Model

The topographical boundary for use in the hydraulic analysis is the east and west levees. The upstream and downstream boundaries are chosen for hydraulic modeling purposes: 1) to allow stabilization of the water surface elevation calculations in HEC-RAS and, 2) to establish consistency with the mathematical boundary conditions between cross section geometries.

Topographic information was located in the USBR rangelines, the 2008 LiDAR DEM, and the 2010 LiDAR DEM. The USBR rangelines were obtained as station-elevation pairs with georeferenced endpoints. Importing the endpoints as linear two-dimensional features within ArcMap allows the conversion of these to three-dimensional features using any DEM followed by comparison to the station-elevation pair data. The 2010 LiDAR DEM is compared directly to the 2008 LiDAR DEM to obtain the highest resolution, continuous terrain. The rangelines verify terrain data and are incorporated into the continuous terrain to supplement for bathymetric data.

The LiDAR-derived terrain data are available as DEM data and raw LiDAR data files. The raw LiDAR files included spatial and descriptive information, enabling classifications to be associated with the spatial location of collection. The river stage at the time of the LiDAR collection measured by the gage allows adjustment of DEM within the river channel to approximate bathymetry. The two surfaces are coupled in ArcMap to generate a single DEM.

The *water* LiDAR classifications are vector points and converted to a raster using the Spatial Analyst tool for the spatial assignment of the channel to the DEM. The "Raster Calculator" tool is used to lower the DEM where there is *water* LiDAR classification coverage. Additionally, the raster is converted to vector polygon for digitizing a number of stream features including the bank lines, land use, and ineffective flow areas. This water classification polygon is also used in defining the overbanks, islands and sand bars for habitat analysis. Basing these features on a single polygon adds consistency to an otherwise discretionary assembly of model features. This terrain model method is summarized in Figure 8.

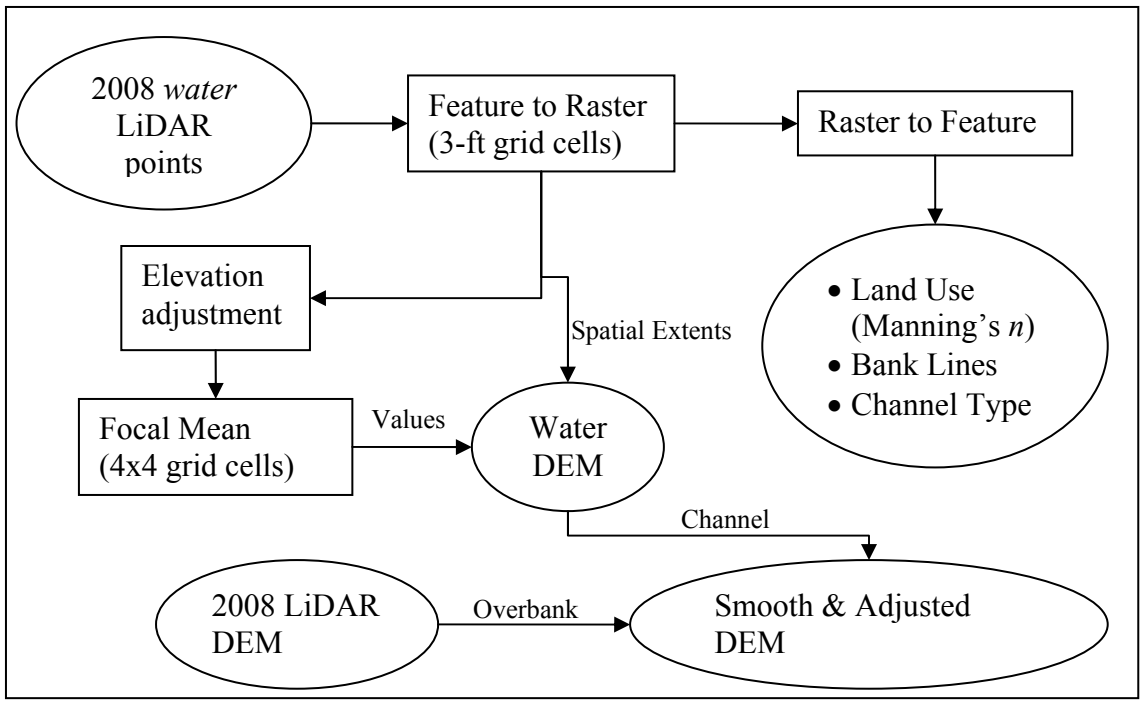

Figure 8: Flow chart for processing 2008 water LiDAR points and 2008 LiDAR DEM into 2008 functional DEM

Hydraulic Model

Geometric data

The stream geometry is assembled with HEC-GeoRAS, the geospatial counterpart to HEC-RAS in ArcMap, using a combination of topography and aerial imagery to digitize hydraulic features. The features digitized in this study include stream centerline, bank lines, flow paths (a combination of the stream centerline and bank lines), cross sections, levees, ineffective flow areas, and the spatial distribution of Manning's *n* values (referred to in the HEC-GeoRAS software as land use).

Stream centerline, bank lines and flow paths. The stream centerline is digitized using the aerial imagery when the channel is at the lowest flow. This is also termed the stream thalwag as it follows the lowest point along the course of flow. The topographical data also helps, but the smoothed channel bottom provides little information compared with the aerial imagery. The stream centerline is used to generate the stationing values of the cross sections and can be considered the coordinate system foundation of the geometric data. The bank lines are digitized in a similar fashion by tracing the outline of the water classification polygon. The stream centerline and bank lines features are copied to the flow paths feature class where these are defined as channel, left bank or right bank.

Cross sections. Cross sections are digitized to represent planes normal to flow to accommodate the one-dimensional nature of HEC-RAS (Ackerman, 2009). As convention they are drawn left to right facing the downstream direction. In many cases cross sections are not straight lines over the entire length, necessitating more than two vertices to remain perpendicular to flow in the main channel and overbank areas. The additional vertices can misrepresent the topography when the overall length is

constructed significantly longer than a straight line perpendicular to the stream flow (Ackerman, 2009). Generally, these errors can be found when the conveyance ratio from one cross section to another is greater than 1.4 or less than 0.7, and a warning is incurred. The solution here is additional cross sections if the geometry cannot be edited to reduce the change in conveyance between cross sections.

Levees. The flow in HEC-RAS does not necessarily follow the stream centerline, bank lines and flow paths. The software computes the water surface elevation directly based on the lowest point on the cross section. In many cases this is inappropriate, such as in the cases of perched channels, near canals, or behind floodwalls. In the case of the Rio Grande, large portions of the irrigation canals paralleling the river are lower than the channel bed and separated by levees. In the HEC-RAS software, the term *levee* is similar but does not necessarily have the same connotations as in flood protection. In the software these features are used to contain the flow first to the proper side of the levee, i.e., computing the water surface to the right of the levee on the left overbank and to the left of the levee on the right overbank, and may in fact indicate roads or merely high ground.

Ineffective flow areas. These features are areas in which the velocity of the water in the downstream direction is close to zero. They are included in the storage calculations but are not included in the wetted perimeter for flow calculations (Brunner, 2010a). They are digitized two-dimensionally in GIS using HEC-GeoRAS based on vegetation identified in the aerial photography and the water classification polygon. The height is calculated from the terrain using HEC-GeoRAS. In HEC-RAS the two-dimensional area per cross section of ineffective flow areas are defined by the ineffective

flow area left and right stations, the ineffective flow area elevation, and the cross section geometry. The ineffective flow area elevation value is determined in HEC-GeoRAS to be the maximum of the left and right stations where the ineffective flow area intersects the cross section (Ackerman, 2009).

Sand bars and islands commonly increase in the density of vegetation towards the middle and decrease towards the edges, therefore the computed ineffective flow area elevation value is not necessarily representative of the volume which will stagnate due to vegetation even if the ineffective flow areas are digitized tightly around places of dense vegetation. Additionally, one ineffective flow area elevation value is assigned per cross section in HEC-RAS which necessitates a thorough analysis to determine the most representative value.

Based on the nature of HEC-RAS using a single elevation per ineffective flow area on each cross section, several procedural steps are necessary to determine the value which is representative of each real-world feature. The portion of each cross section having one or more ineffective flow areas are analyzed using the ArcMap tools "Feature Vertices to Point," "Clip," and "Surface Spot" to determine the representative height for use in the ineffective flow area feature. The cross sections are converted to points at intervals determined by HEC-GeoRAS and the grid cell size of the DEM using "Feature Vertices to Point," the points not within ineffective flow areas are removed using "Clip," and the elevation of these points are tabulated in the attribute table using "Surface Spot." These data are analyzed in Excel to determine the maximum elevation of ineffective flow area per cross section. In Excel, the elevation data were increased by this value and

imported into the Cross Section Ineffective Flow Area's Elevation table in HEC-RAS directly.

Land use. The land use features represent the spatial variation of Manning's *n* values. This feature has to be a single-part polygon feature without overlapping edges and, unlike many of the other hydraulic features, it may intersect the cross section as many times as necessary. The use of the spatially distributed Manning's *n* values allows capturing the prevalence of numerous sand bars and islands in the Rio Grande through the LLHR reach. The water classification polygon defined the Manning's *n* values in the land use feature class.

Boundary conditions

Slope. HEC-RAS requires information for at least one cross section per reach to begin computations. Several types of information are available: known water surface elevation, critical depth, normal depth (requiring additional information on reach slope), and rating curve (pairing stage and flow). The normal depth boundary condition is most appropriate based on known data. For this, the downstream slope is determined; slope on the upstream cross section is not a necessary parameter in HEC-RAS when using a subcritical flow regime (Brunner, 2010a). The downstream slope is analyzed in Excel after utilizing the ArcMap 3D Analyst tools to convert the two-dimensional digitized stream centerline feature to three dimensions. First, the normal depth is calculated using an adaptation of Manning's equation which solves for depth using either trial and error or a nonlinear algebraic equation solver (Sturm, 2010):

$$AR^{2/3} = \frac{A^{5/3}}{P^{2/3}} = \frac{nQ}{\mathrm{K}\sqrt{\mathrm{S}}} \qquad \text{Equation 15}$$

where:

A = cross sectional area of flow

R = hydraulic radius

P = wetted perimeter

n = Manning's hydraulic roughness coefficient

Q = flow

K = conversion factor, 1.49 for U.S. Customary units (cfs)

S = channel slope

For a rectangular channel of width b and normal depth y_n this simplifies to:

$$\frac{(by_n)^{5/3}}{(b+2y_n)^{2/3}} = \frac{nQ}{K\sqrt{S}} \qquad \text{Equation 16}$$

Second, the critical depth is found using the Froude number equation set equal to one (Sturm, 2010) as:

$$F_R = 1 = \frac{V}{g\sqrt{D}} \qquad \text{Equation 17}$$

where:

F_R = Froude number

V = velocity

D = hydraulic depth

For a rectangular channel of critical depth, y_c, Equation 17 is rewritten as:

$$y_c = \left[\frac{Q}{b\sqrt{g}}\right]^{2/3} \qquad \text{Equation 18}$$

Equation 16 and 18 are solved to determine the normal and critical depths, respectively. Then the depth of flow measured at the nearest gage is compared to these values to determine the boundary condition in HEC-RAS between normal or critical depth.

Flow regime. The critical component of HEC-RAS is the amount and type of flow to be modeled. The software requires at least one location where the flow rate is known. Based on the engineering design of the LLHR project, flows of 1,000 cfs (28 cms), 2,500 (71 cms), and 5,000 (142 cms) were defined at the upper-most cross section. Each is modeled as a separate steady flow regime to better address any errors, warnings and notes encountered.

Utilizing the daily average gage data available online (USGS, 2010d) for the long-term station USGS 08330000 Rio Grande at Albuquerque, NM, probabilities of occurrence for these specified flow rates are computed. Descriptive statistics are calculated for average daily discharge data from the first year after flow regulation by Cochiti Dam through the end of the calendar year 2009. These data provide information on the design flows in terms of the overall frequency of flow at the LLHR site.

Critical shear stress

Equation 6 is used to determine the grain Reynolds number. One of the critical Shields parameter equations (Equations 12 through 14) are selected for use based on the grain Reynolds number. Equation 11 is then used to determine the critical bed shear stress. Accepted values for the fluid properties of water are found in numerous texts including Munsun, Young, and Okiishi (2006) and utilized in the appropriate equations. Sediment studies have included those by Nordin and Beverage (1965), Ho et al. (2010) and USGS (2010c) to determine the grain properties of density and size distribution typical of those in the Middle Rio Grande.

Data Analysis and Results

Topography

The most recent USBR rangelines within the project area were collected in 2005, approximately three years after the construction of the project. The endpoints were used to generate a two-dimensional line feature in ArcMap for conversion to a three-dimensional feature using the LiDAR DEM terrain. In most cases, the overbank station-elevation data are very close to the 2008 LiDAR DEM. In a number of cases, the channel is not clearly defined in the rangeline station-elevation data. The primary use of the USBR rangelines is to integrate bathymetry into the DEM. However, the rangeline station-elevation data is not of sufficient quality nor spaced closely enough to improve bathymetry. The USBR rangeline comparison with the 2008 LiDAR DEM and the 2010 LiDAR DEM is presented in Figure 9. This USBR rangeline is representative of the geometry of the LLHR and is located at the upstream end of the project site. It includes the western boundary of the LLHR site, the root wad berm.

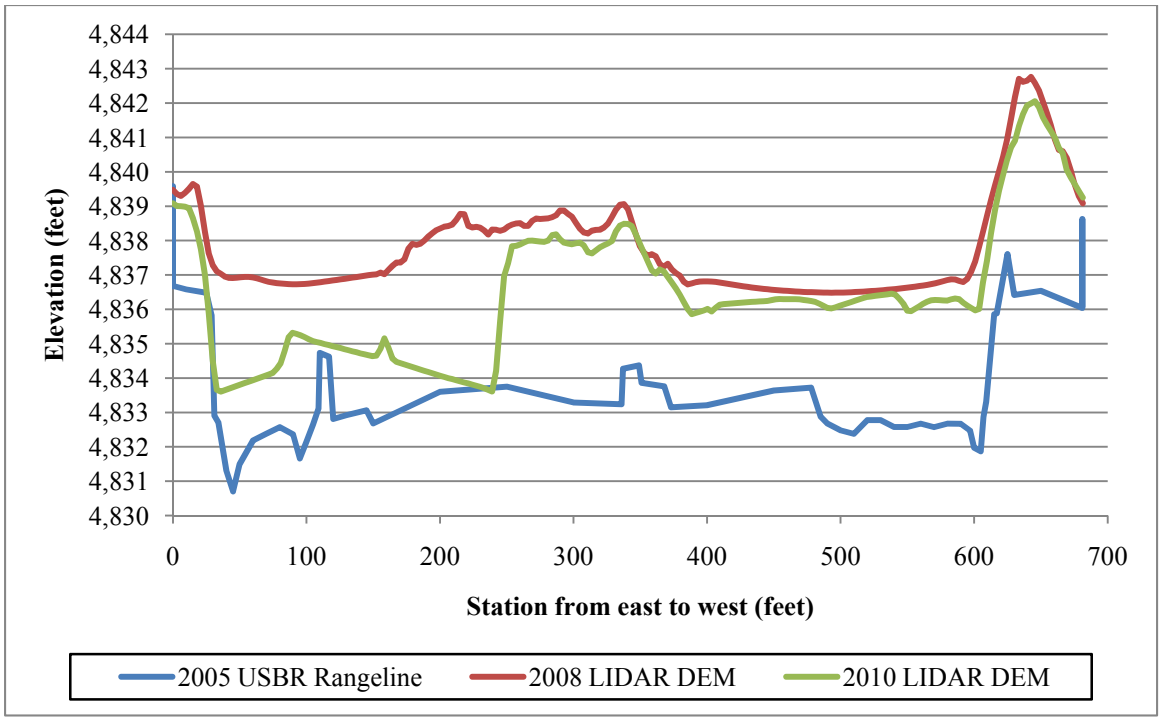

Figure 9: Comparison of available topographic and bathymetric data using one representative rangeline IS-772

The density of the 2008 LiDAR sensor detections indicates very detailed terrain analysis. The average spacing of LiDAR collections classified as *ground* is 2.4 ft while *water* has an average spacing of 1.7 ft. This is likely due to *vegetation* classification alongside the *ground* classifications, while *water* classifications are more spatially homogeneous and inherently more reflective. The 2008 LiDAR collections for a representative area of the LLHR project are shown in Figure 10.

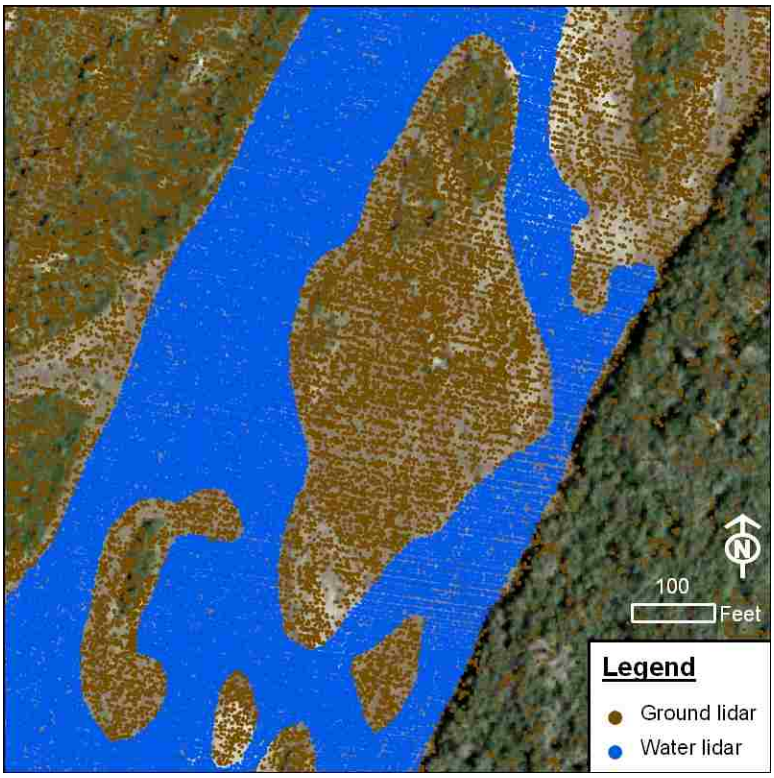

Figure 10: LiDAR collections near the downstream side channel

The 2010 LiDAR DEM shows less resolution than the 2008 LiDAR DEM. Investigation into the point spacing shows that the 2010 LiDAR sensor detections of *ground* classifications were approximately 5.5 ft on average with minimum less than one foot and maximum spacing of 77.6 ft. The 2010 LiDAR DEM shows a grid cell spacing of 3 ft, the same as the 2008 LiDAR DEM, although it appears derived from a coarser terrain model. The comparison between the two DEMs is presented in Figure 11.

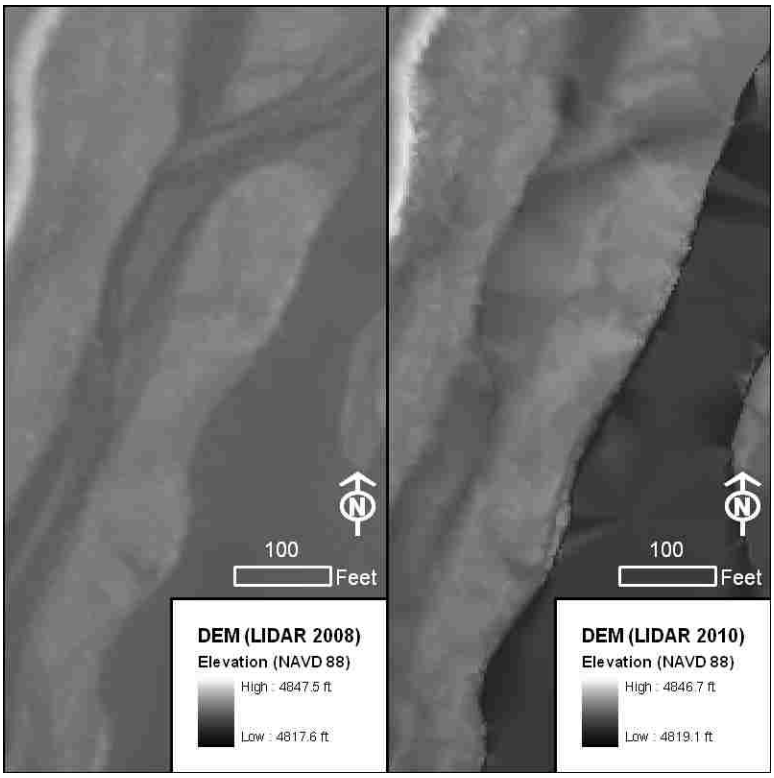

Figure 11: Comparison of LiDAR DEM terrain data, both of same scale and extent, showing differing resolution

The comparative analysis of the USBR rangelines, the 2008 LiDAR DEM and the 2010 LiDAR DEM shows that the 2008 LiDAR DEM is better suited for use in this study. The integration of the USBR rangelines is not shown to improve the bathymetry for hydraulic modeling. The 2010 LiDAR DEM has less spatial resolution than the 2008 LiDAR DEM and is not included in this study. The 2008 LiDAR DEM and its adjusted derivative are the sole terrain datasets discussed forward in this study.

Initial investigation of the 2008 LiDAR data classified as *water* show three occurrences of collection; and comparison of these to local gage data indicate significant change in water surface elevation. The calibration of the LiDAR data includes hydraulic modeling of the terrain adjacent to the gage yielding a correlation of LiDAR data to

measured river stage or information supporting a decision to remove LiDAR classified as *water*.

Geoprocessing of the LiDAR indicates that the DEM included the channel area as an interpolated surface from the banks, that is the *ground* points along the banks were used to interpolate across the area identified as *water* to produce a continuous surface. Utilizing the points classified as *water* to generate the spatial domain of bathymetric extent, a global elevation shift applied to these data will allow incorporation of a relatively flat channel bottom into the terrain model. The complete modeling of the main channel bottom is not necessary as the overbank features are the main concern. The original DEM is shown in Figure 12 along with an elevation profile across the stream channel and LLHR project.

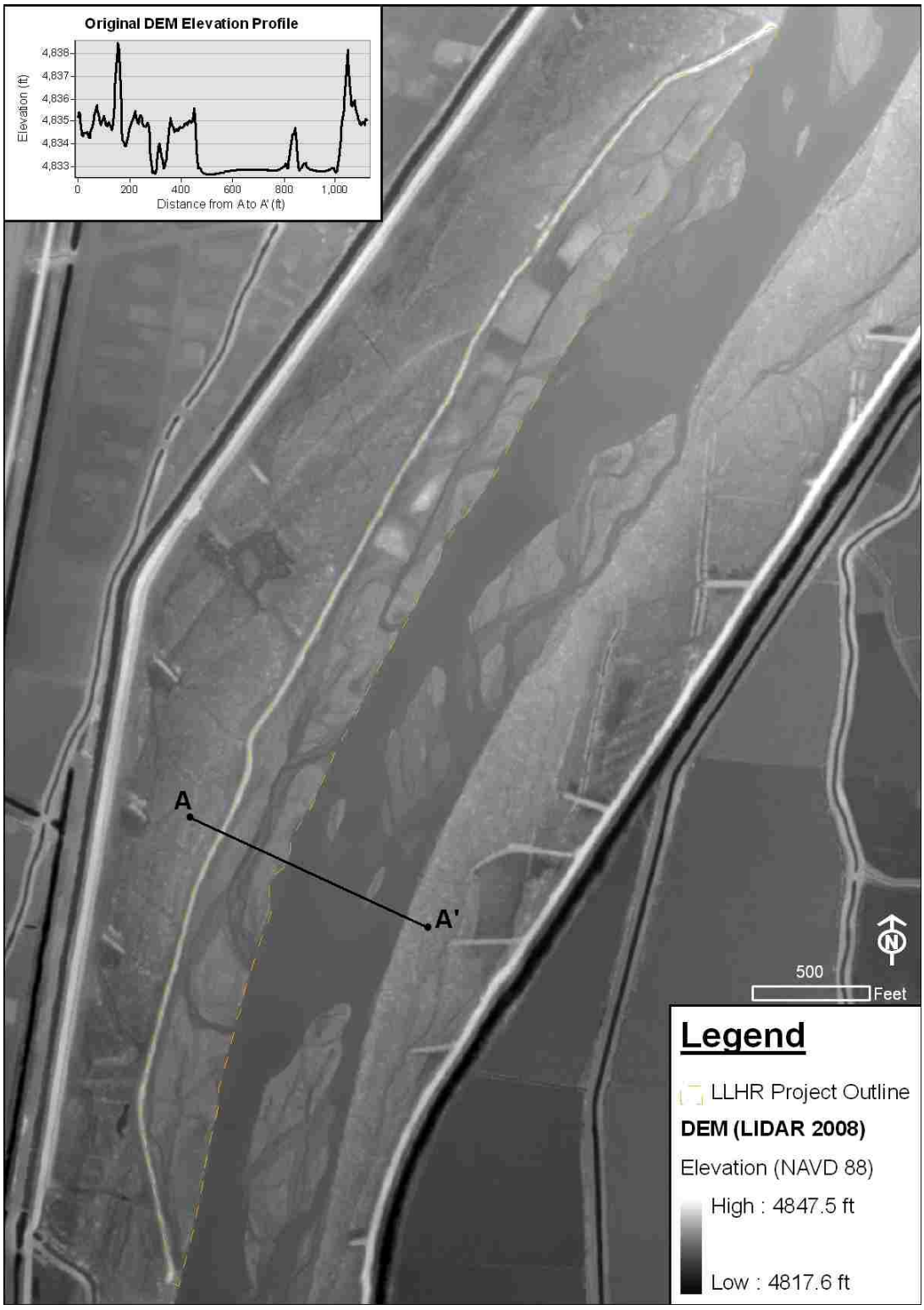

Figure 12: Elevation profile across the stream channel, from A to A′, using the original DEM based on the 2008 LiDAR

The GIS attribute data for each *water* detection point was exported to an Excel spreadsheet to analyze the date and time of the collections in terms of river stage. An adjoining sheet within Excel contained the 15-minute stage data from the Bosque Farms USGS gage. The USGS rating curves for each site are used to determine the stage at zero flow, i.e. the stage datum. The Bosque Farms gage rating curve showed a zero-flow height datum of 12 ft. The Excel function "LOOKUP" was used in the LiDAR spreadsheet to determine the stage at which each LiDAR point was collected. The daily minimum, maximum, and average for both stage and depth values were calculated using Excel, and are shown in Table 2. Each day shows a range of less than one-tenth of a foot (0.03 m) in stage values and the entirety of the LiDAR collection shows a range of 0.6 ft (0.18 m) in stage values. The depth is interpreted as the stage minus the datum height and averages for all LiDAR collections.

Date	Number of LiDAR Collections	Minimum of Gage Stage (ft)	Maximum of Gage Stage (ft)	Average of Gage Stage (ft)
3/2/2008	139,015	15.93	15.95	15.937
3/3/2008	38,790	15.89	15.89	15.890
3/8/2008	274,572	15.32	15.33	15.329

Table 2: Summary attributes of stream stage at the time of LiDAR collection showing a less than one-tenth of a foot difference in stream stage per day and six tenths of a foot overall

The extent to which the DEM is adjusted is based on investigation of the aerial imagery and *water* classifications in which two conditions exist: 1) coverage by *water* LiDAR points, and 2) presence of water in aerial imagery. Those areas covered by *water* LiDAR classifications, and appear to be water in the aerial imagery, are adjusted

downward by the average depth of 3.6 ft (1.1 m). Areas covered by *water* LiDAR points but do not appear to be water in the aerial imagery are adjusted downward by 1.8 ft (0.55 m). These are shown in Figure 13.

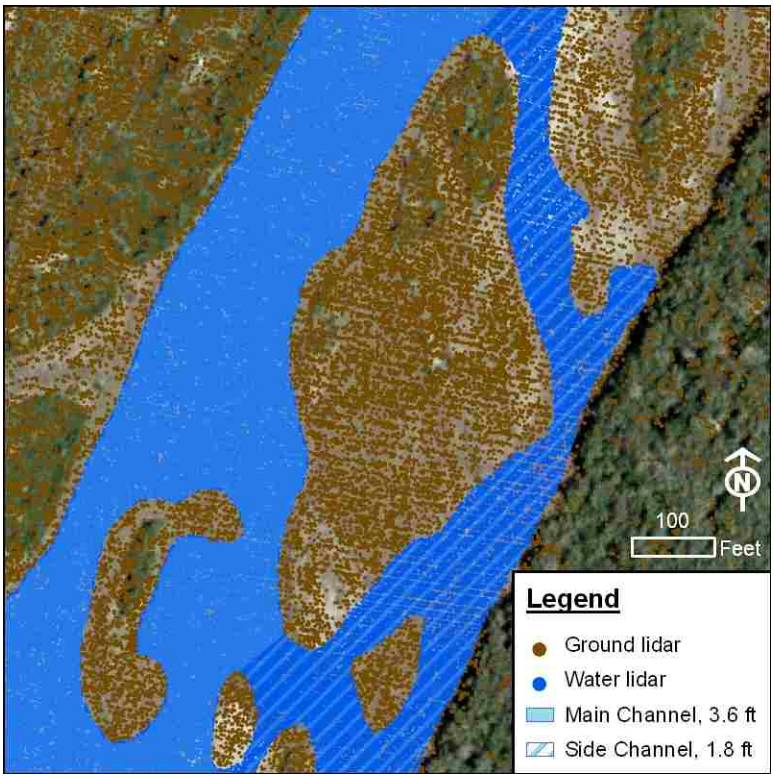

Figure 13: LiDAR collections and associated terrain adjustment for channel bathymetry

The dense spacing of the *water* LiDAR points allows a direct conversion of this point vector shapefile into a raster grid having the same 3 ft grid cell size as the DEM using the ArcMap Spatial Analyst tool "Features to Raster." To generate a relatively smooth channel bottom and fill any gaps, the raster is processed using the "FocalMean" function within the ArcMap Spatial Analyst Raster Calculator. This function returns the mean of surrounding grid cells for each grid cell in a raster. For this analysis, the eight adjacent grid cells were used to generate a mean value for each grid cell.

Before the elevation values are adjusted the channel types are determined. The FocalMean raster grid is converted to a polygon shapefile. This shapefile is edited to digitize the boundaries of channel types and attributed with the appropriate adjustment value, i.e. the amount of adjustment to the DEM being either 3.6 or 1.8 ft. This Channel Type polygon is shown in and used later to define the spatial extent of Manning's *n* values in HEC-GeoRAS. The Channel Type polygon is converted back to a raster using the adjustment value as the grid cell value. The Adjustment raster grid is then subtracted from the FocalMean raster grid to generate an adjusted DEM with a more complete bathymetry suitable for hydraulic modeling. This DEM is shown in Figure 14.

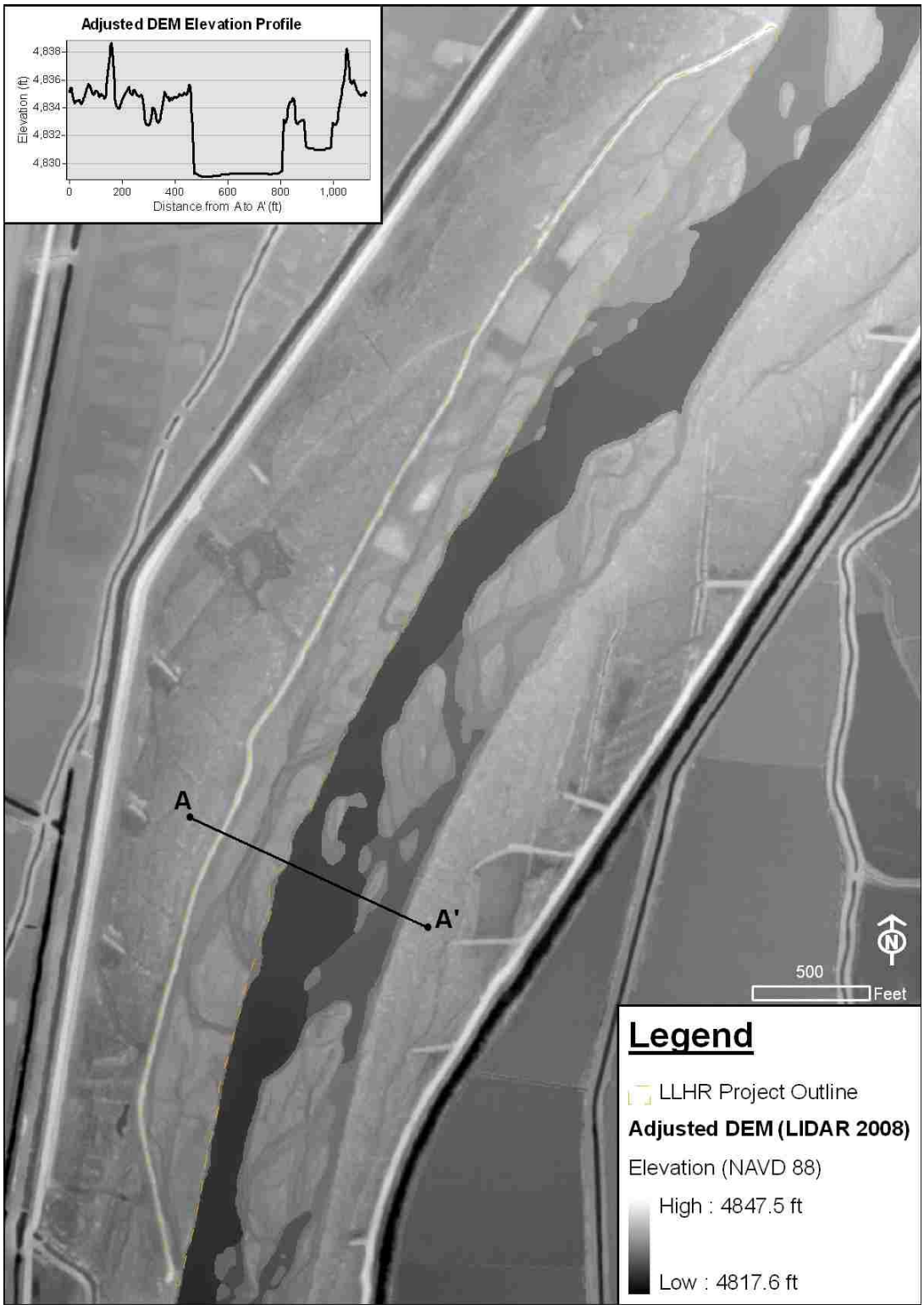

Figure 14: Elevation profile across the stream channel, from the same A to A′ as Figure 12, and LLHR project using the adjusted DEM based on the 2008 LiDAR and an estimation of channel bathymetry

Boundary conditions

Flow regime

Descriptive statistics (Table 3) were calculated for average daily discharge data from the first year of flow regulation by Cochiti Dam (1974) through the end of calendar year 2009 (13,129 values). These statistics show a positive skewness value which indicates the data are skewed to the right by some high values. The statistics of the $\log_{10}$-transformed values of daily discharge data were computed to reduce the positive skew.

Table 3: Descriptive statistics of daily discharge data in cubic feet per second for USGS Gage 08330000 Rio Grande at Albuquerque, NM, January 1, 1974, through December 31, 2009

Mean	1,299
Median	782
Mode	1,030
Standard Deviation	1,369
Skewness	2.13
Minimum	2
Maximum	8,650
Count	13,129

Transforming the daily discharge data using the $\log_{10}$ function yields a lower skew value (Table 4). This $\log_{10}$-transformed skewness value is slightly negative, indicating a less asymmetrical shape to a normal distribution curve than the original, untransformed daily discharge data.

Table 4: Descriptive statistics of $\log_{10}$-transformed daily discharge data for USGS Gage 08330000 Rio Grande at Albuquerque, NM, January 1, 1974, through December 31, 2009

Mean	2.917
Median	2.893
Mode	3.013
Standard Deviation	0.442
Skewness	-0.829
Minimum	0.301
Maximum	3.937
Count	13,129

The mean average daily flow based on the values in Table 4 is 826 cfs versus the 1,299 cfs value in Table 3. Sorting and ranking the daily discharge data allows percentile and exceedance values to be calculated by summation. Table 5 presents the modeled and $\log_{10}$-transformed flow values, modeled flow percentiles and exceedances, and the percent of the data which fall within ±100 cfs of the modeled flow. This 100 cfs value is an arbitrary value based solely on a visual inspection of the ranked and sorted daily discharge data.

Table 5: Percentile and exceedance for each modeled flow, based on counts

Modeled flow (cfs)	Log_{10} of modeled flow	Percentile (%)	Exceedance (%)	Percent of data within 100 cfs (%)
1,000	3	57.4%	42.6%	5.2%
2,500	3.398	86.1%	13.9%	1.4%
5,000	3.699	96.1%	3.9%	0.6%

Note: Percentile is the percent of daily flows at or below the modeled flow value and exceedance is the percent of daily flows above the modeled flow value.

The exceedances of the modeled flows indicate that 57% of average daily flows recorded in the USGS Gage 08330000 Rio Grande at Albuquerque, NM are lower than

the minimum modeled flow of 1,000 cfs (28 cms). Additionally, only 4% of flows exceed the maximum modeled flow of 5,000 cfs (142 cms). Since construction of the LLHR site in 2002, estimated daily average flow at the USGS Gage 08331160 Rio Grande near Bosque Farms, NM has neared or exceeded 5,000 cfs (142 cms) during the years 2008 (5,060 cfs, 143 cms), 2009 (4,710 cfs, 133 cms) and 2010 (5,330 cfs, 151 cms) (USGS, 2010f). In June of 2005, daily average flow of 6,510 cfs (184 cms) was recorded at the USGS Gage 08330000 Rio Grande at Albuquerque, NM (USGS, 2010d).

This analysis implies that the 1,000 cfs (28 cms) value is fairly common in the record and the 5,000 cfs (142 cms) value is not. Limitations of this analysis are that the flows were recorded at a different location than the LLHR site and that, for the short period of overlapping records, the USGS Gage 08330000 Rio Grande at Albuquerque, NM experiences higher flows than the USGS Gage 08331160 Rio Grande near Bosque Farms, NM due to agricultural and municipal diversions in addition to the attenuation of flow as it moves downstream.

Slope

ArcMap 3D Analyst was used to extract station-elevation data for analysis in Excel. Over the entire length of the LLHR hydraulic model reach the slope is 0.0009 ft/ft. The higher slope over the downstream quarter-mile of the LLHR reach is due to being one of three major drops in the bed elevation. The bed elevation profile, from downstream to upstream, is shown in Figure 15.

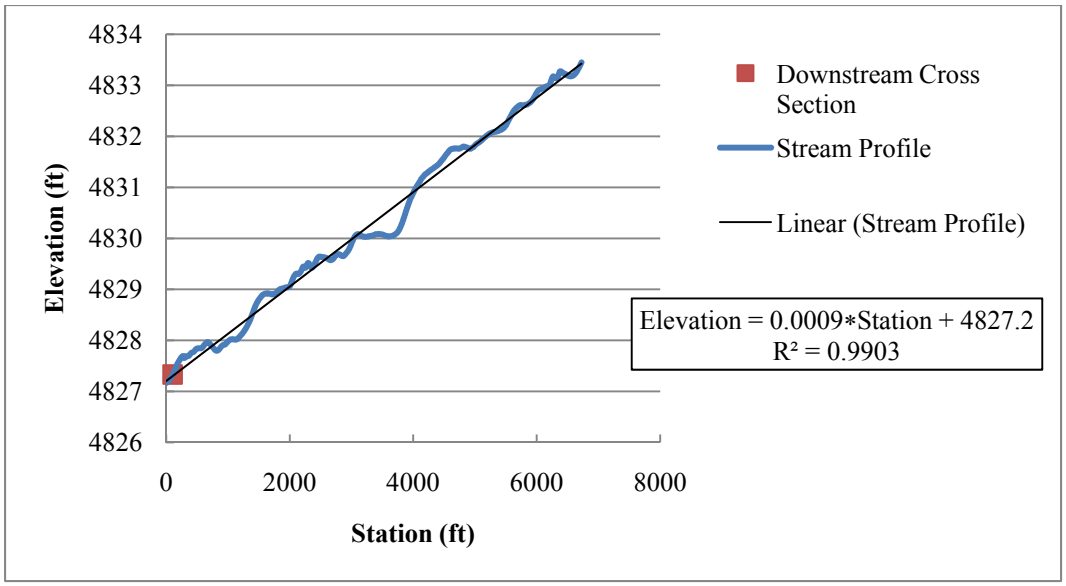

Figure 15: Slope of the Rio Grande in the LLHR reach with elevation measured above mean sea level and station measured from downstream to upstream

A reach 50 ft upstream and 50 ft downstream of the farthest downstream cross section was chosen as representative of the slope at that cross section. Analysis shows that the slope is 0.0023 ft/ft at the downstream boundary of the HEC-RAS model, as shown in Figure 16.

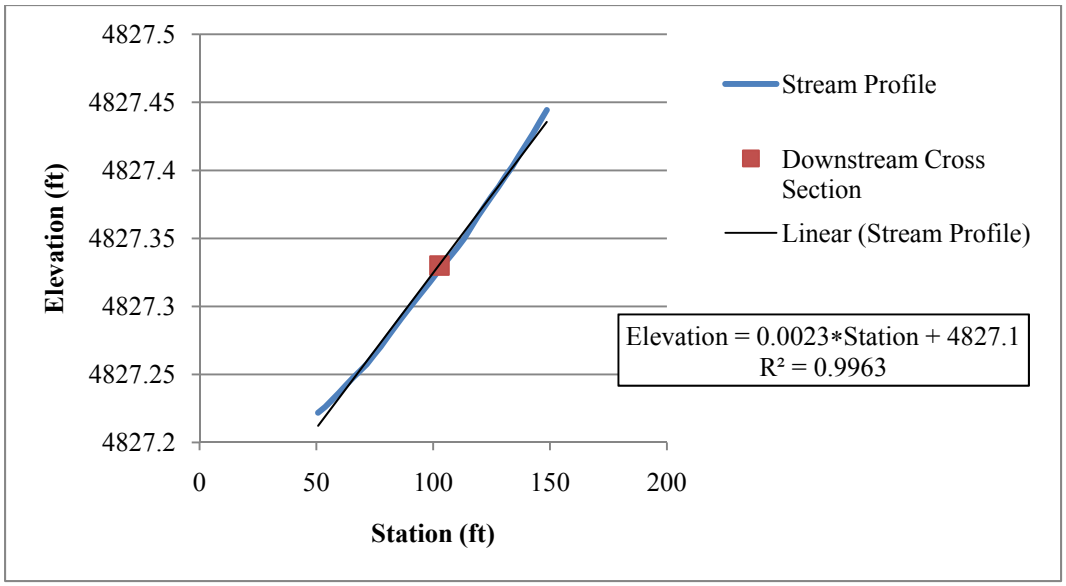

Figure 16: Slope of the Rio Grande stream bed profile along a 50 ft length upstream and downstream of cross section at station 102.702 ft, the downstream boundary of the HEC-RAS model

Hydraulics

Geometric data

The stream centerline was digitized using the DEM to best approximate the river thalwag. A total of 76 cross sections were placed with an average spacing along the digitized stream centerline of 84.6 ft with the minimum spacing of 36.2 ft and the maximum spacing of 188.6 ft. Bank lines and Land Use (Manning's *n*) were digitized based on the water classification polygon. The west bank levee was the root wad berm and the east levee was digitized using overbank elevations. Ineffective flow areas were digitized using aerial imagery. These features are shown in Figure 17.

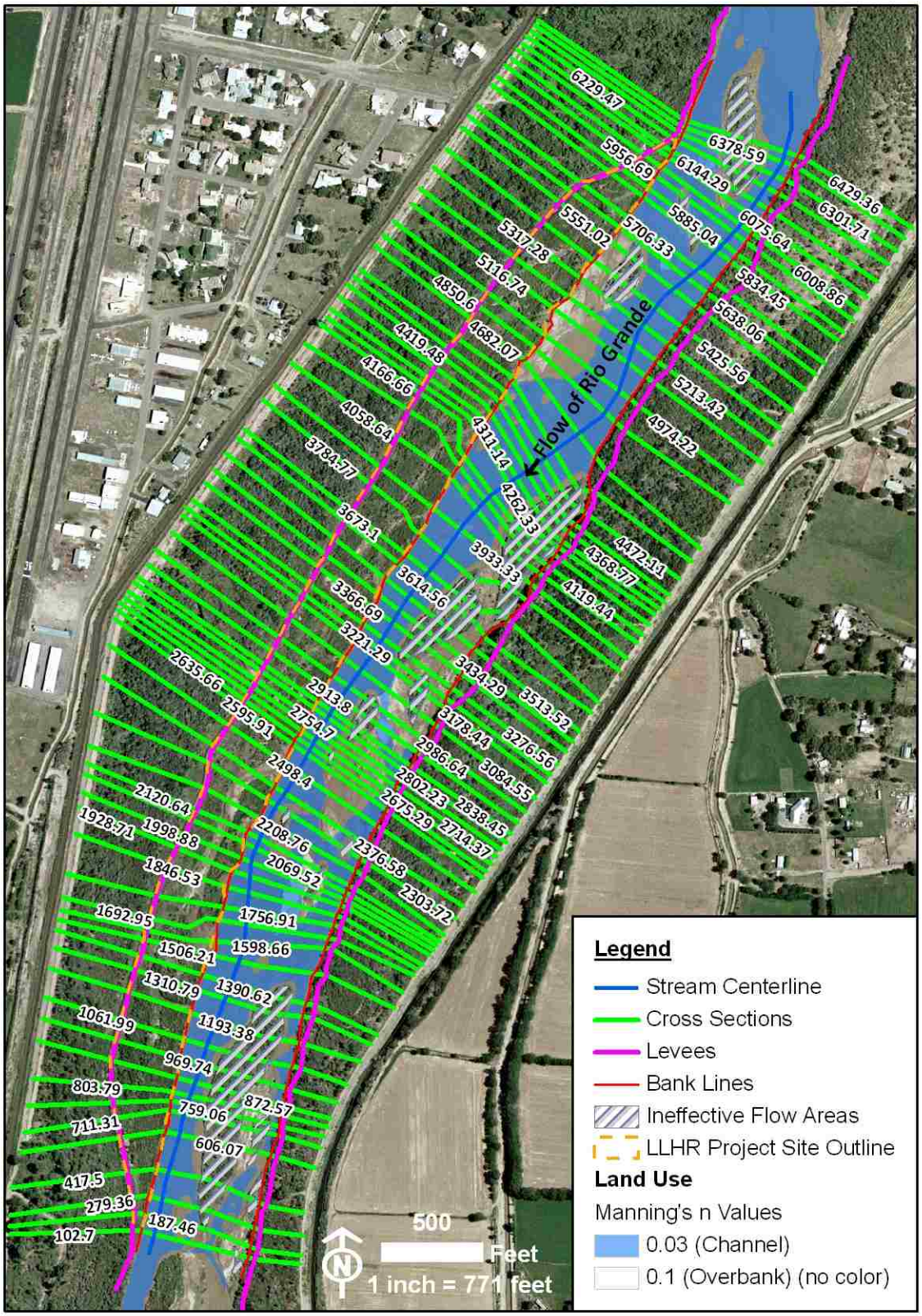

Figure 17: HEC-GeoRAS features in ArcMap with cross sections labeled with station

Bed material

Based on USGS (2010c) data collected for dry-sieved samples of bed material collected at the USGS 08330000 Rio Grande at Albuquerque, NM gage, the grain size distribution shows a d_{50} of approximately 0.014 in (0.35 mm), shown in Figure 18. This shows good agreement between the sampling periods closest to the LiDAR collection.

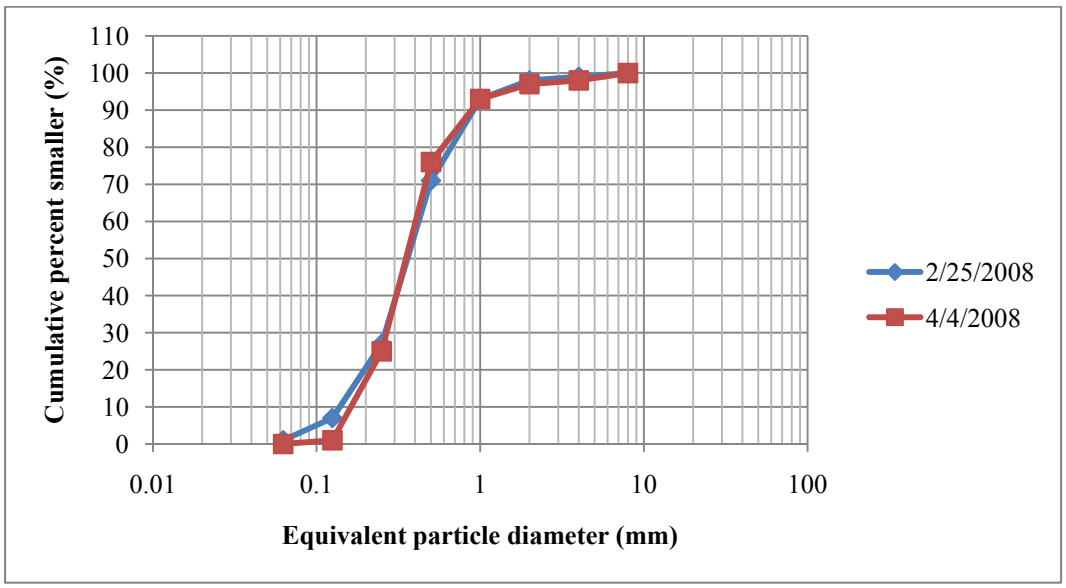

Figure 18: Grain size distribution of bed material measured by the USGS at stream gage 08330000 Rio Grande at Albuquerque, NM, at sampling times closest to LiDAR collection

The bed material is classified under the American Association of State Highway and Transportation Officials (AASHTO) as granular material A-3, a sand having no more than 10% silt and clay material (Das, 2006). The Unified Soil Classification System uses d_{10}, d_{30}, and d_{60} values to determine coefficients of uniformity and curvature. The equation for the coefficient of uniformity is d_{60} / d_{10} and the equation for the coefficient of curvature is $d_{30}^2 / (d_{10} * d_{30})$ (Das, 2006). Determining from the USGS (2010c) data a

value for d_{10} of 0.15 mm, a d_{30} of 0.27 mm, and a d_{60} of 0.41 mm, the coefficients of uniformity and curvature are found to be 2.73 and 1.185, respectively. The bed material is thus classified as SP, poorly graded sand or gravelly sand with less than 5% fines according to the Unified Soil Classification System (Das, 2006).

Critical shear stress

The shear stress is calculated within HEC-RAS and mapped using HEC-GeoRAS within ArcMap. Comparing the shear stress mapping results to the critical bed shear stress value yields a mapping of locations where the habitat features are unstable, either from deposition where shear stress is less than the critical value or from erosion where it exceeds the critical value.

The nearest temperature sampling periods closest to the LiDAR collection were at the time of the bed sediment samplings, with 7°C on 2/25/2008 and 10°C on 4/4/2008 (USGS, 2010c). Water has a specific weight of 62.40 lb/ft^3 (9.802 kN/m^3) at 7°C and 62.41 lb/ft^3 (9.804 kN/m^3) at 10°C (Munsun, et al., 2006). Additionally, water has a kinematic viscosity of 1.543 x 10^{-5} ft^2/s (1.434 x 10^{-6} m^2/s) at 7°C and 1.406 x 10^{-5} ft^2/s (1.307 x 10^{-6} m^2/s) at 10°C (Munsun et al., 2006). Based on the equations and the nature of these fluid properties, the values which would produce a more conservative critical shear stress are 62.40 lb/ft^3 (9.802 kN/m^3) and 1.543 x 10^{-5} ft^2/s (1.434 x 10^{-6} m^2/s), respectively, which are both properties of water at 7°C.

Nordin and Beverage (1965) assumed the specific weight of sand in the Middle Rio Grande near Belen, New Mexico, to be 5.14 slugs/ft^3 or 165 lb/ft^3 (25.9 kN/m^3) which yields 1.65 for the submerged specific weight of the bed sediment. A specific gravity of 2.65 is commonly assumed for sand and may have lead to the Nordin and

Beverage assumption of 5.14 slugs/ft^3. Ho et al. (2010) utilized a specific weight of sand in the Middle Rio Grande near Albuquerque, New Mexico, of 168 lb/ft^3 (26.4 kN/m^3) which yields 1.69 for the submerged specific weight of the bed sediment. Ho et al. (2010) utilized a median sediment diameter of 0.02 in (0.51 mm) which is nearly 40% larger than the 0.014 in (0.35 mm) median sediment diameter found in this study. The 1.65 value for the submerged specific weight of the bed sediment is applied here.

The grain Reynolds number is determined from Equation 6 to be 18.32. The appropriate equation for the critical Shields parameter calculation is Equation 13, and its value is determined to be 0.04637. Equation 11 then yields the critical bed shear stress as 0.0055 lb/ft^2 (0.262 Pa). This is the threshold value used to determine if the median bed material is in motion.

Hydraulic model

Flow regime

Numerous sand bars and islands make direct measurements of channel width in ArcMap an overestimate and likely inaccurate, however, the USGS Gage 08331160 Rio Grande near Bosque Farms, NM, is located in an ideal location. Here there are neither bars nor islands and clearly defined banks allow measurement of the channel width in ArcMap. The channel width measured in ArcMap is 300 ft (79 m), the aerial imagery obtained when flows were 804 cfs, the representative slope of 0.0009 ft/ft, and a Manning's *n* value of 0.03 are used to calculate a normal depth of 1.42 ft (0.43 m) using Equation 16. With these same data, the critical depth calculates to 0.47 ft (0.14 m) using

Equation 18. The normal depth is greater than the critical depth, thus the slope is determined to be mild (Sturm, 2010), and the flow regime set to subcritical in the HEC-RAS model.

Manning's *n* values

Values for hydraulic roughness, Manning's *n*, were spatially varied with differing values for the exposed sand bed and the vegetated areas. Manning's *n* values for the Rio Grande have been studied and calibrated with 0.03 being most representative. Based on site inspection and vegetation surveys (Siegle & Reed, 2007) the dominant plant type is characterized as a tall and slender shrub with a woody stem, i.e. cottonwood saplings, willows, and saltcedar. The Manning's *n* value for the vegetated areas is set to 0.1. The Channel Type polygon generated in the Topography section is used here to define the spatial extent of Manning's *n* values within the HEC-GeoRAS model assembly.

Ineffective flow areas

Based on visual inspection by myself, sand bar and island vegetation is primarily composed of grasses with some willow species. The depth of stagnation is expected to be approximately 3 ft (0.9 m).

Cross section points filter

The high resolution of the DEM produces detailed cross sections with more station-elevation pairs than is allowed by the HEC-RAS software. The maximum number of station-elevation pairs per cross section is 500. In the Geometry Editor of HEC-RAS, the "Cross Section Points Filter" tool is used to remove points one at a time

down to a user-specified number by eliminating those which produce the least change in area of the cross section.

Summary errors, warnings and notes

The HEC-RAS software is designed to find the best results based on the input data and flags many computations which fall outside conventional parameters. Errors are those that prohibit the program from completing the computations; warnings provide information that the hydraulic results may be unreasonable; and notes provide information on how the software is performing computations. Warnings are most useful as they imply how the model can be improved, such as with a warning that conveyance ratios are outside tolerance indicating that cross sections may be spaced too far apart.

Mapping

Hydraulics

The HEC-RAS results are imported into ArcMap using HEC-GeoRAS. These data are the water surface extents and water depths for each flow profile; the flow distributions for velocity; shear stress values; and geometry data for stream centerline, user defined cross sections, reach lengths, bank stations, levees, ineffective flow areas and Manning's *n* values. Each are processed one-by-one by HEC-GeoRAS.

Inundation mapping. The water surface extents for each flow profile computed in HEC-RAS are imported to ArcMap as two-dimensional points and the ArcMap triangulation method is used to generate a water surface from the three-dimensional cross sections in the form of a triangulated irregular network (TIN) with each node of the water

surface TIN defined by the intersection of the water surface extent on the cross section (Ackerman, 2009). The TIN is converted to a water surface DEM grid for comparison to the terrain DEM grid. For each of the cells in the grids, where the water surface DEM is higher than the terrain DEM, the terrain DEM is subtracted from the water surface DEM to produce the water depth grid.

At the lowest flow rate of 1,000 cfs (28 cms), the flows do not enter the overbank area and are confined to the channel, some sand bars, and inlets along the stream banks. The modeled flow rate of 2,500 cfs (71 cms), shows extensive inundation of the LLHR project overbank area. Numerous sites in the side channels are inundated to depths up to 3 ft (0.9 m). The 2,500 cfs (71 cms) depth map is shown in Figure 19. The HEC-RAS model shows that at the highest flow rate of 5,000 cfs (142 cms), nearly the entire project area including areas on the eastern overbanks are inundated. There are four major areas of high ground in the project site which remain above the water surface.

Inundation on the eastern overbank is controlled using user-defined levee features along the bank line features. Mapping of this inundation is unrealistic in most cases, as the water surface profile extends across the entire cross section if these levee features are overtopped.

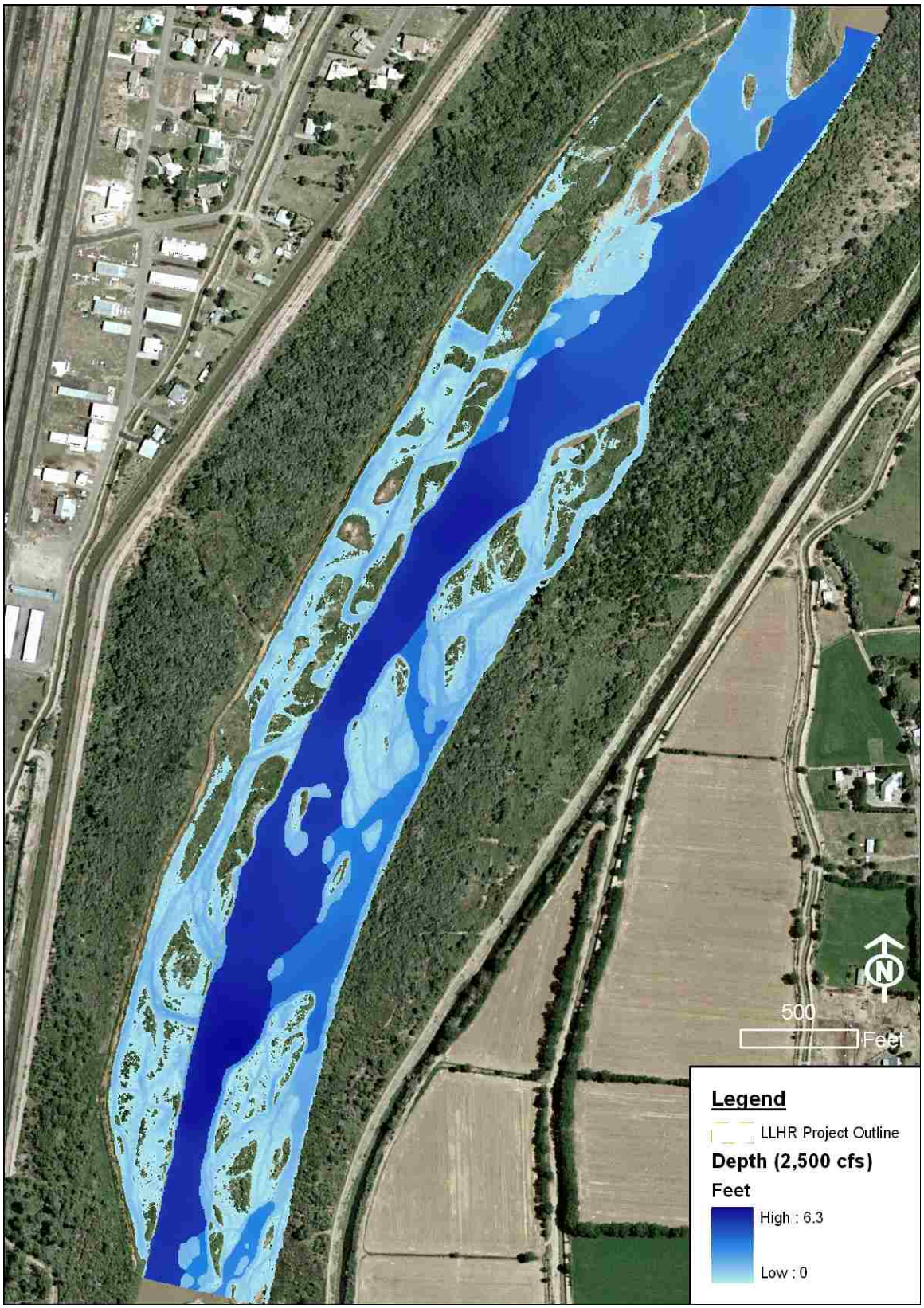

Figure 19: Depth map for the 2,500 cfs flow regime

Velocity mapping. Velocities mapped for the 1,000 cfs (28 cms) flow profile show the narrow portions of the stream channel achieving 3.5 ft/s (1.1 m/s) and wider areas around 1.5 ft/s (0.5 m/s). The 2,500 cfs (71 cms) flow profile has very similar velocities with the narrow and wide portions at the same 3.5 ft/s (1.1 m/s) and 1.5 ft/s (0.5 m/s), respectively, as shown in Figure 20. The 5,000 cfs (142 cms) flow profile peaks at 9.3 ft/s (2.8 m/s) in the narrow portions and approximately 2.3 ft/s (0.7 m) in the wider portions. It should be noted that HEC-RAS and HEC-GeoRAS do not predict two-dimensional flow around objects (Ackerman, 2009) such as islands. The one-dimensional velocity can be compared between adjacent cross sections upstream and downstream of features which impact the cross section geometry.

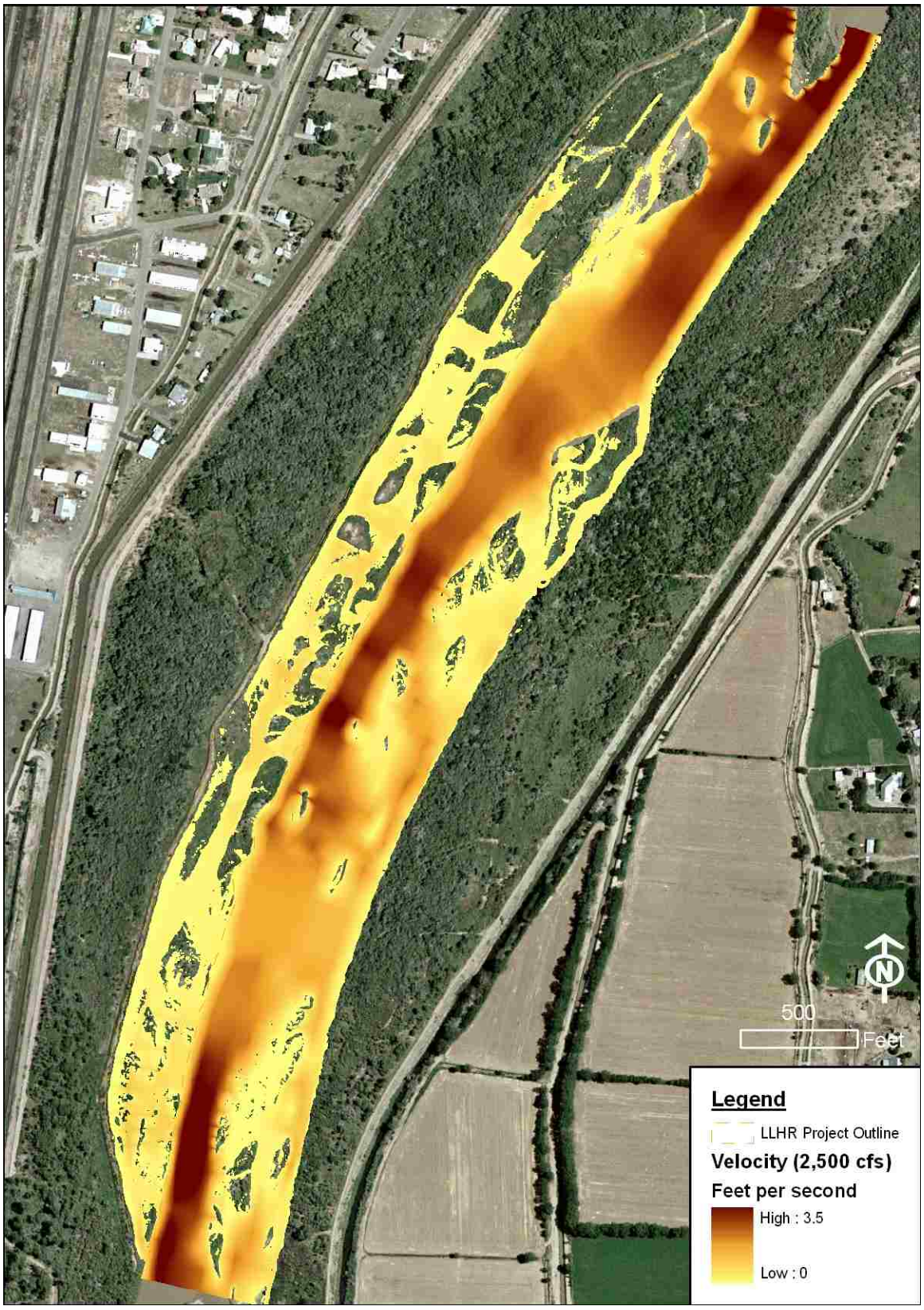

Figure 20: Velocity map for the 2,500 cfs flow regime

Shear stress mapping. Shear stresses mapped in the LLHR project overbank area show a maximum of 0.26 lb/ft^2 (12 Pa) for the 2,500 cfs (71 cms) flow regime, and a maximum of 0.75 lb/ft^2 (36 Pa) for the 5,000 cfs (142 cms) flow regime. These are greater than the critical bed shear stress of 0.0055 lb/ft^2 (0.262 Pa) for the median diameter bed material, 0.014 in (0.35 mm) sand. Shear stress mapped over the entirety of the hydraulic model for the 2,500 cfs flow regime shows a maximum of 1.25 lb/ft^2 (60 Pa), occurring in the main channel. Shear stress mapped for the 5,000 cfs (142 cms) flow regime shows no areas with less than the critical bed shear stress of 0.0055 lb/ft^2 (0.262 Pa). The shear stress map for the 2,500 cfs flow regime, with values scaled above and below the critical shear stress value, is shown in Figure 21.

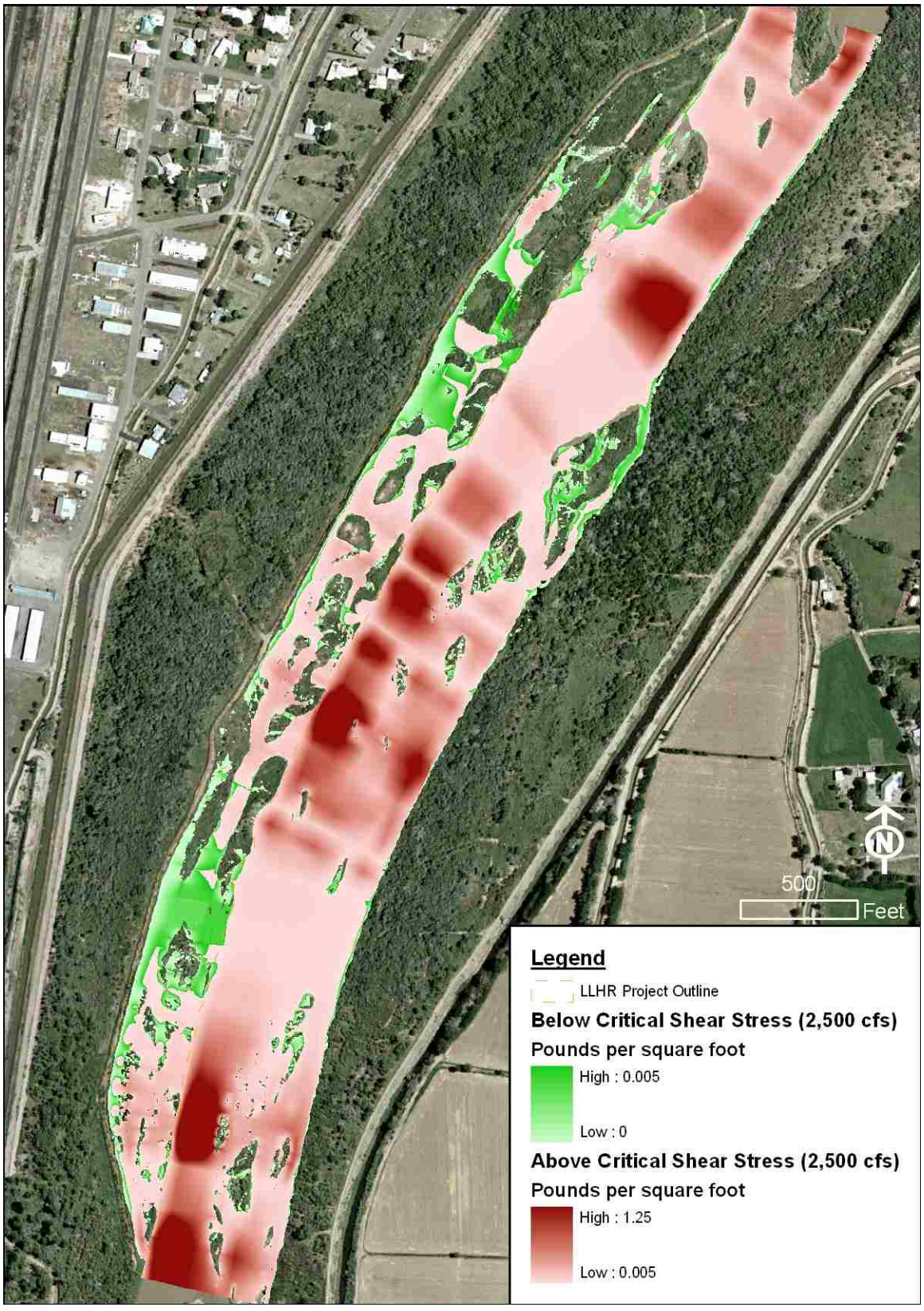

Figure 21: Shear stress map for the 2,500 cfs flow regime

Habitat

Pairing and joining data. The frequency of use data paired to depth and velocity data developed by Dudley and Platania (1997) are joined to the hydraulic model results in ArcMap. The hydraulic results are converted from raster to vector points for two reasons: 1) the joining of two data fields in one raster is cumbersome in ArcMap, and 2) the Spatial Statistics tools available in ArcMap are designed for data in vector form. The Spatial Join tool is used to generate one point shapefile with both depth and velocity data per point. The frequencies defined in Dudley and Platania (1997) are in bins of 3 cm for depth and 3 cm/s for velocity, therefore the hydraulic data is converted from U.S. Customary units to metric units and rounded to the nearest bin in the shapefile attribute fields. Rounding to the nearest bin is a simple Field Calculation in the attribute table using the "Integer" function. Similar attribute fields are added to both the point shapefile and the frequency of use table defining the depth and velocity pairs in text format (i.e., 42 cm depth and 9 cm/s velocity are paired to read "42,9"). Using the "Table Join" tool, the frequency of use data are matched and joined to the hydraulic model data. For example, the pair "42,9" is matched to and joined by the 24.2% frequency of use. One shapefile feature class is populated with depth, velocity, and frequency of use at each point based on hydraulic modeling and statistical habitat frequency of use.

The results indicate that habitat is plentiful within the LLHR project site transverse channels, low velocity side channels, bank inlets, and overbank areas. The total area of the LLHR project site is 41 acres with 20.6 acres of those classified as having greater than zero percent frequency of use. The edges of many instream sand bars also showed high habitat potential. For the 2,500 cfs (71 cms) flow regime shown in

Figure 22, the north side channel and its backwaters show high habitat frequency of use values. These backwaters have extensive and contiguous areas of high habitat frequency of use values. The southern side channel is a focal point for habitat providing a hydraulically connected corridor of high frequency of use values. The northern end of this south side channel has a backwater with the largest contiguous area of maximum frequency of use values. The downstream portion of the south side channel also shows an above average concentration of habitat frequency of use values. The downstream south side channel overbank area shows high habitat frequency of use values although these are less hydraulically connected than the main south side channel.

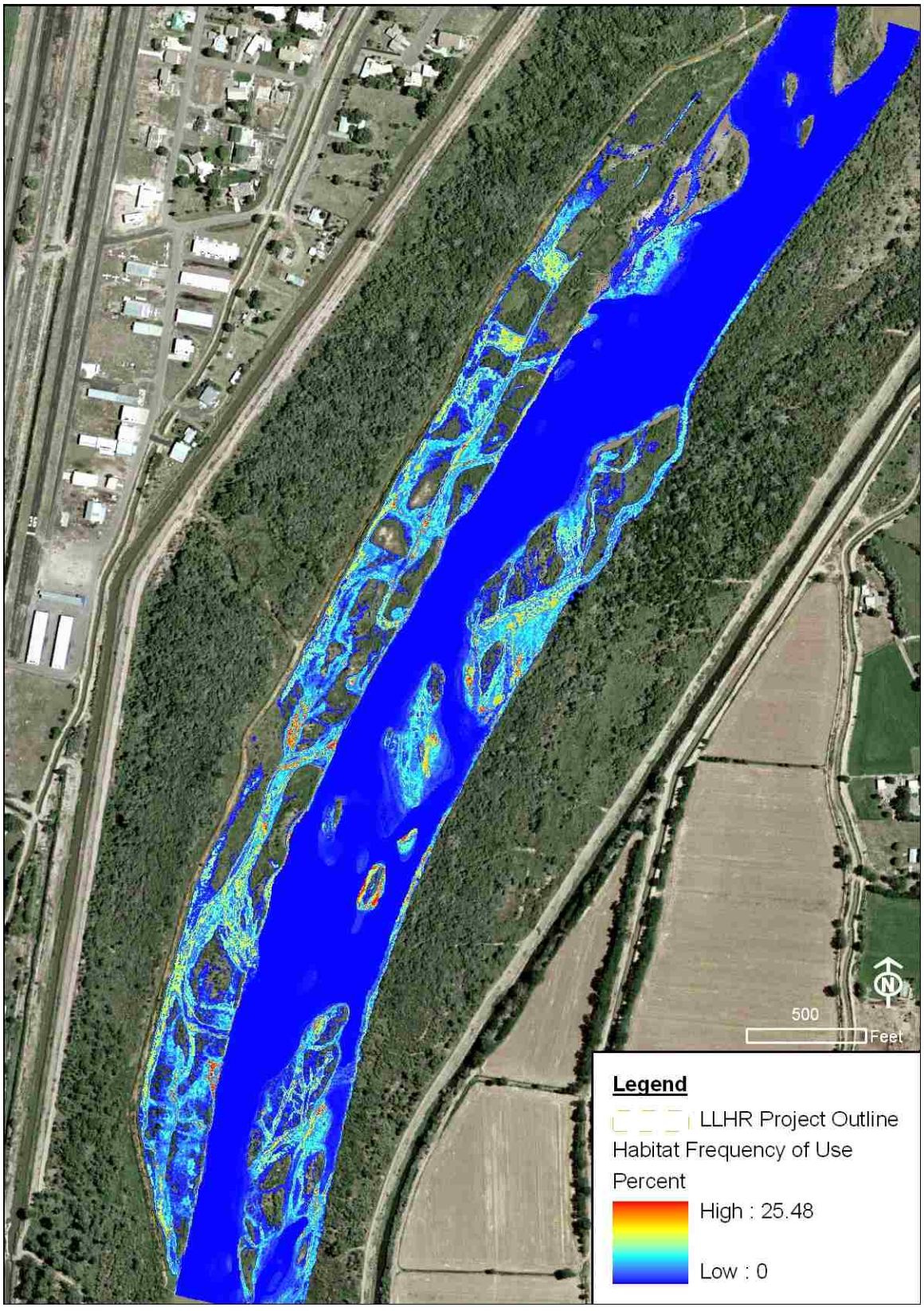

Figure 22: Habitat percent frequency of total use for the 2,500 cfs flow regime

Spatial statistics

Spatial statistics were performed at the global and local scales. Global results are more objective and show a similar distribution of statistically significant habitat frequency as the raw habitat frequency mapping. The local results are less objective as they must be separated into hydraulically related groups to obtain local statistics. ArcMap tools for local spatial statistics define the local neighborhood by distance in a circular radius. The habitat features are engineered for hydraulic connectivity and have linear geometries. Neighborhoods are digitized based on a relationship of hydraulic connectivity and local spatial statistics are analyzed by these neighborhoods.

Standard score. The global statistics analysis utilizes the standard score, also known as a Z Score, which computes the number of standard deviations each value is above or below the mean in a data population. Each habitat use frequency value is given a Z Score based on the mean and standard deviation of the global data. The equation for the Z Score is $(x - \mu) / \sigma$ (Spiegel, Schiller, & Srinivasan, 2000). Here x is the value for which the Z Score is calculated, μ is the population mean, and σ is the population standard deviation. The mean and standard deviation of the habitat frequency of total use values are found in the raster properties dialog of ArcMap to be 3.36 and 4.76, respectively. The Field Calculator is used to calculate Z Scores for each point. The results are shown in Figure 23.

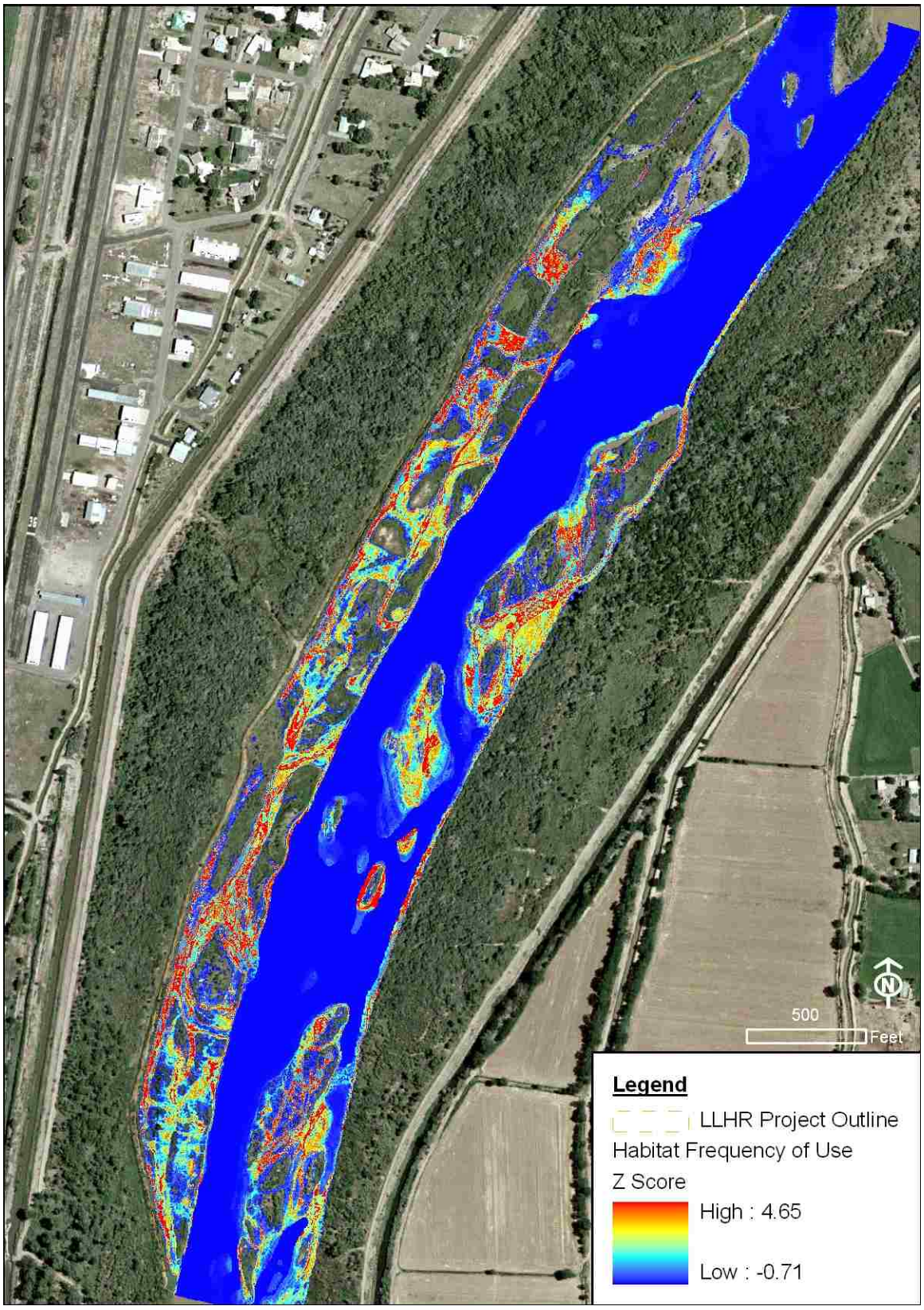

Figure 23: Statistical standard scores for habitat frequency of total use for the 2,500 cfs flow regime

Hot Spot analysis. The "Hot Spot Analysis" tool compares each value to its surrounding values to determine significance (ESRI, 2009). The local set of neighboring features are compared to the global set of features and when the local values are higher or lower than expected based on global statistics a statistically significant Z Score results (ESRI, 2009). A large positive Z Score indicates a dense clustering of high values and a large negative Z Score likewise indicates a clustering of low values. The "Hot Spot Analysis" tool incorporates the Getis-Ord Gi* Z Score, based on the standard Z Score and developed to include a spatial correlation and distance weight for applications in a GIS environment (Getis & Ord, 1992). The tool requires a distance band to determine the spatial domain of 'local' which can be determined using the "Calculate Distance Band from Neighbor Count" script in Spatial Statistics Toolbox under the Utilities Toolset. This tool shows that the neighbor count of 12 results in a distance band of 6.5 ft (1.98 m), as shown in Figure 24. The documentation of the "Hot Spot Analysis" tool in ArcMap states that, as a general rule, no less than eight neighbors should be included in the analysis for each point (ESRI, 2009).

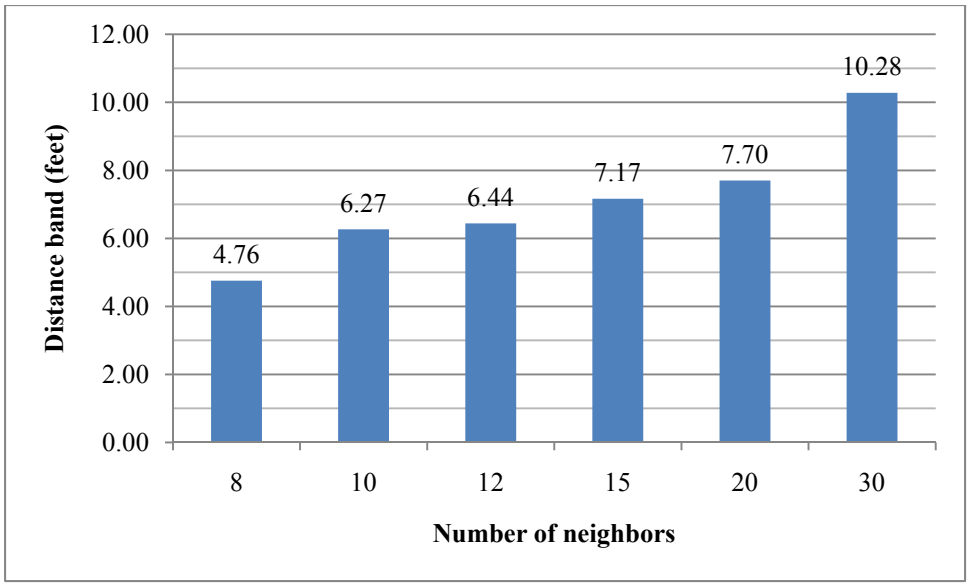

Figure 24: Results from the "Calculate Distance Band from Neighbor Count" tool showing the rationale for the use of 6.5 feet as the distance band in the "Hot Spot Analysis" tool

The "Hot Spot Analysis" tool is located in the Spatial Statistics Tools under the Mapping Clusters Toolset. Also available is the "Hot Spot Analysis with Rendering" tool under the Rendering Toolset which automatically renders the layer symbology and saves this as a layer file; the two are otherwise identical. These results are shown in Figure 25.

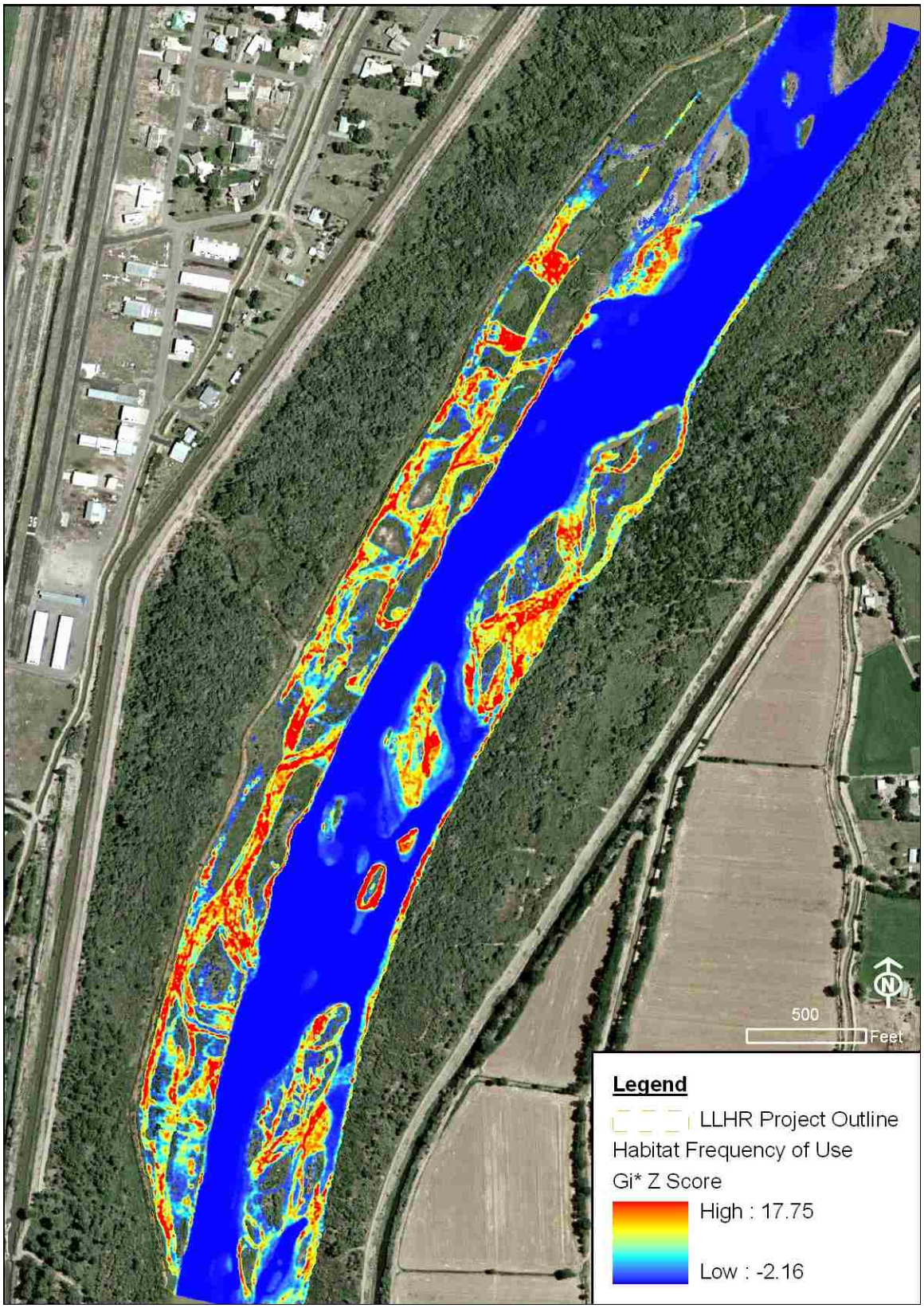

Figure 25: Hot Spot Analysis of the habitat frequency of total use for the 2,500 cfs flow regime

Comparison of statistical analyses. The three statistical methods are presented side-by-side for comparison in the area of the downstream side channel (refer to Figure 6) in Figure 25. It is seen that the "Gi* Z Score" map indicates a higher density of preferential habitat compared to the "Percent of Total Use" map. This is likely an overstatement as the "Percent of Total Use" map is a direct measure of habitat preference and each value above zero indicates preferential habitat. It should be noted that zero values for habitat frequency of use are statistical probabilities of capturing minnows and not necessarily areas having hydraulic properties which are detrimental to the minnow. The "Standard Score" map shows a moderate density of habitat in relation to the other two maps.

The spatial statistics agree with recent monitoring which shows that the LLHR site provides lateral, floodplain habitat and shallow water with reduced velocity (Hatch & Gonzales, 2010). Importantly, the site includes backwater habitat which reduces "downstream displacement of eggs and larvae," a characteristic vital to the survival of the endangered species (Hatch & Gonzales, 2010, p. 31).

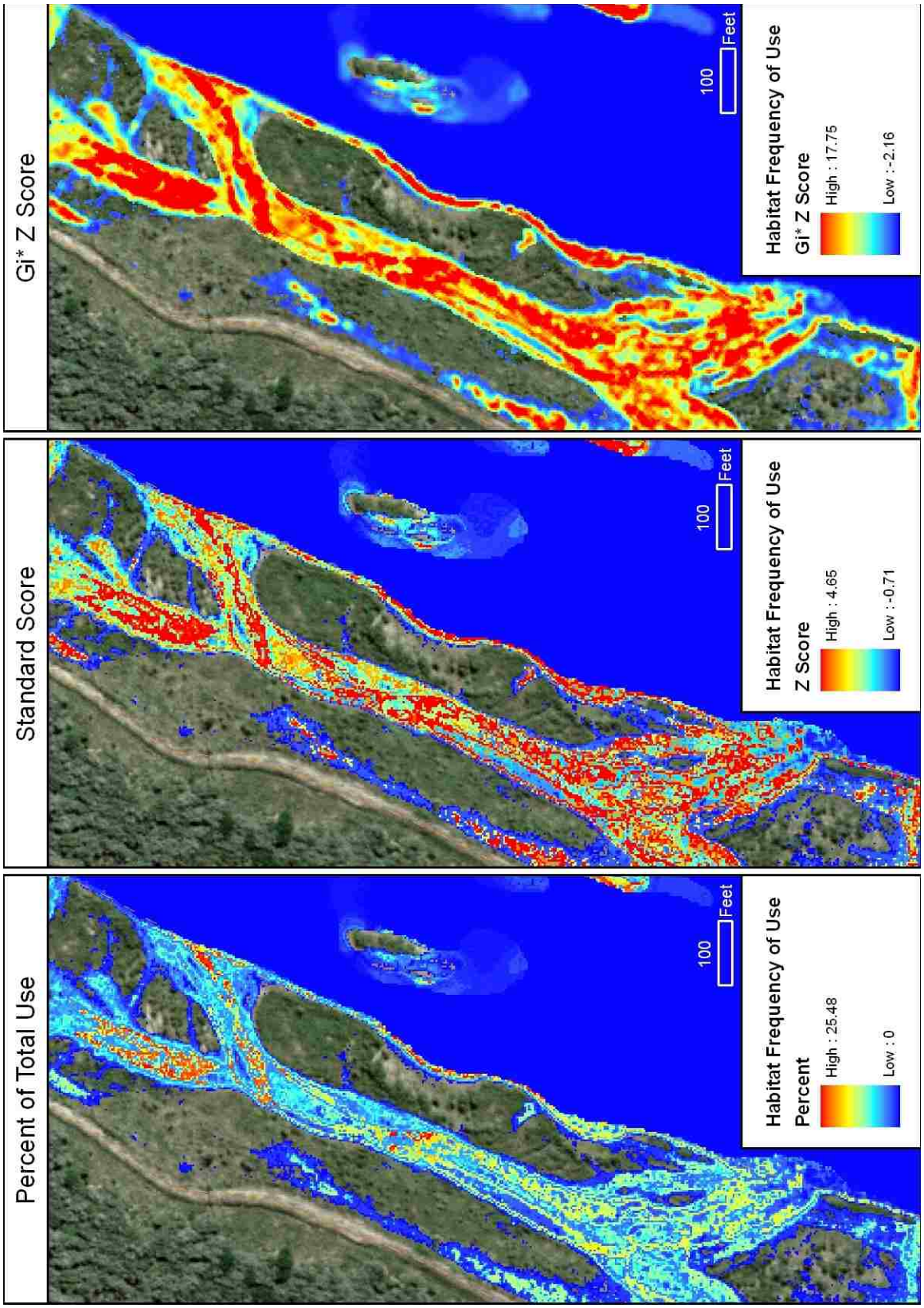

Figure 26: Habitat comparison map

Discussion

Hydraulic model

The hydraulic model was relatively straightforward to assemble and execute once the input data were assembled and processed. Assuming that the terrain data are prepared with an understanding of cross section geometry and spacing, another researcher could assemble and execute this model. That said, the model has serious shortcomings including the fundamental limitation of one-dimensional calculations. Was this study to focus on instream habitat alone, such as pools, riffles, runs, and bends, the HEC-RAS software may be sufficient. The lack of bathymetry was an additional limitation of this study. Software capable of two- or three-dimensional hydraulic calculations would be ideal for a study which includes overbank inundation. Numerous studies presented here have shown that the one-dimensional nature of the HEC-RAS calculations overestimate the area and depth of inundation.

Geospatial analysis

Visualization of the results in a GIS such as ArcMap allows seamless transition from hydraulics to geospatial analysis. Once in ArcMap the hydraulic results are available to an incredible array of analysis tools which can be combined in any manner and provide powerful and reproducible analysis techniques. The results of these analyses can then be visualized and shared in highly detailed plots.

Endangered species habitat

Based on the results from the hydraulic modeling and geospatial analyses, the LLHR site has extensive areas where depth and velocity are in the favorable range for the minnow. More than half of the total acreage of the LLHR project site is found to have greater than zero habitat frequency of use values. The instream sand bars, transverse channels, low velocity side channels, and overbank areas all experience inundation to depths and with velocities that are favorable habitat for the minnow and allow its movement from the channel into and between these habitat features. The downstream side channel in particular shows substantial habitat potential with extensive clusters of maximum habitat frequency of use values. An important observation is that several natural, non-engineered, instream sand bars and islands on the eastern side of the channel also show high habitat frequency of total use values, Z Scores and Gi* Z Scores.

The exclusion of nonnative and invasive vegetation types does influence the long term habitat quality in that fully grown cottonwoods and willows will continue to tolerate yearly inundation while shading the water to provide cooler water temperatures which are preferable to the minnow. The results indirectly support increases in flycatcher habitat from restoration activities at the LLHR. Dense willow stands provide quality nesting and breeding habitat for the flycatcher. Although the species prefers native vegetation, nonnative and invasive vegetation types are also utilized. Although saltcedar has reestablished in small quantities at the LLHR site, it is not an impediment to the flycatcher and the saltcedar is likely isolated to corners of the LLHR site not frequently inundated.

Habitat sustainability

The critical bed shear stress required to initiate sediment mobility is exceeded in several locations by the maximum shear stress mapped with HEC-GeoRAS. This indicates sediment is both eroded and deposited throughout the LLHR project site. Depending on the spatial balance of erosion and deposition, two scenarios under the 2,500 cfs (71 cms) flow regime are possible: 1) gradual erosion of restoration features resulting in increasing depths and velocity during inundation events beyond the preferable range of the minnow; and 2) gradual deposition of sediment resulting in the overbank area becoming hydraulically disconnected from the main channel. The 5,000 cfs (142 cms) flow regime shows the entirety of the site experiencing shear stress higher than the critical shear stress threshold indicating that future conditions are likely to exhibit the erosion of habitat features.

The revegetation of the site also poses a risk to the unsustainable accumulation of sediment. Thick stands of cottonwood and willow saplings increase the hydraulic resistance to flow, thereby decreasing velocity and increasing depth. This will cause sediment accumulation over time.

Conclusions and recommendations

This study successfully incorporated hydrologic investigation, digital terrain modification, hydraulic modeling under various flow regimes for several parameters, geospatial analyses of hydraulic results in relation to biological parameters, and visualization of each process and its analytical result. This study introduces a novel approach to the civil and hydraulic engineering analysis of stream habitat restoration. These methods can be applied at all stages of a project: in the design phase to compare plans, as part of a post-construction report to validate effectiveness, and to provide cost-effective monitoring for years after project completion. These methods can be applied to diverse project types and locales to examine the habitat quality of a completed or proposed project, or to collect baseline habitat quality information for a specific site.

The LLHR site is found to be a successful attempt in engineering critical habitat for two endangered species. The return of an inundation regime to the site is shown to strengthen the ecology of native species, and that of the endangered flycatcher, in addition to controlling the spread of non-native and invasive species. It is also found to have provided these benefits over time and is likely to remain a sustainable source of habitat for both species into the near future. Additional maintenance is necessary as the project experiences sediment erosion and deposition over time.

This study was limited by the lack of bathymetric information. In light of the additional expense to collect these data, LiDAR sampling efforts should correspond to times when the flow is at its minimum, during the months from July to October, in order to maximize the spatial extent of LiDAR collections of *ground* classifications. LiDAR sampling during late autumn months after much of the foliage has fallen, allows LiDAR

signal penetration into the thick bosque cover to provide increased resolution of the vegetated areas. Unfortunately, the timing of the minimum flows (late summer irrigation season) and the lack of foliage (winter) do not necessarily overlap. Collection efforts could potentially occur during October when flows are low and some foliage has fallen, or in November when flows are slightly higher than in October but most foliage has fallen. The most optimal course of action is separate LiDAR collections: one solely of the channel during the lowest flows in July and one of the overbank during winter months. Limited funds are common with projects such as these, therefore a compromise weighted towards the LiDAR collection of channel features is preferred over the collection of overbank features. Algorithms which interpolate terrain features under canopies are becoming more common and reliable, while the interpolation of bathymetry in a highly variable sand bed river is neither.

Future hydraulic studies focusing on overbank habitat should utilize the numerous two- and three-dimensional hydraulic modeling software packages. The additional cost is justified with the increase in hydraulic engineering accuracy and the detail available in the geospatial environment. Two software packages are currently available free of charge from the National Center for Computational Hydroscience and Engineering at the University of Mississippi. These packages, CCHE2D and CCHE3D, are marketed as utilizing geospatial information but this author cannot comment on the similarities to the ease of use available with HEC-GeoRAS.

Bibliography

Ackerman, C. T. (2009). *HEC-GeoRAS, GIS Tools for Support of HEC-RAS using ArcGIS User's Manual Version 4.2* (Report CPD-83). Retrieved from United States Army Corps of Engineers, Hydraulic Engineering Center website: http://www.hec.usace.army.mil/software/hec-ras/documents/HEC-GeoRAS42_UsersManual.pdf

Brunner, G. W. (2010a). *HEC-RAS River Analysis System Hydraulic Reference Manual Version 4.1* (Report CPD-69). Retrieved from United States Army Corps of Engineers, Hydraulic Engineering Center website: http://www.hec.usace.army.mil/software/hec-ras/documents/HEC-RAS_4.1_Reference_Manual.pdf

Brunner, G. W. (2010b). *HEC-RAS River Analysis System User's Manual Version 4.1* (Report CPD-68). Retrieved from United States Army Corps of Engineers, Hydraulic Engineering Center website: http://www.hec.usace.army.mil/software/hec-ras/documents/HEC-RAS_4.1_Users_Manual.pdf

Bash, J. S., & Ryan, C. M. (2002). Stream restoration and enhancement projects: Is anyone monitoring? *Environmental Management*, 29(6), 877-885. DOI: 10.1007/s00267-001-0066-3

Bates, P. D., Marks, K. J., & Horritt, M. S. (2003). Optimal use of high-resolution topographic data in flood inundation models. *Hydrological Processes*, 17, 537-557. DOI: 10.1002/hyp.1113

Bovee, K. D., Lamb, B. L., Bartholow, J. M., Stalnaker, C. B., Taylor, J. G. & Henriksen, J. (1998). *Stream habitat analysis using the Instream Flow Incremental Methodology*. (Information and Technology Report USGS/BRD-1998-0004). Fort Collins, CO: U.S. Department of the Interior, Geological Survey, Biological Resources Division Information and Technology.

Cao, Z., Pender, G., & Meng, J. (2006). Explicit formulation of the Shields diagram for incipient motion of sediment. *Journal of Hydraulic Engineering* ,132(10), 1097-1099. DOI: 10.1061/(ASCE)0733-9429(2006)132:10(1097).

Casas, A., Benito, G., Thorndycraft, V. R., & Rico, M. (2006). The topographic data source of digital terrain models as a key element in the accuracy of hydraulic flood modelling. *Earth Surface Processes and Landforms*, 31, 444-456. DOI: 10.1002/esp.1278

Castellarin, A., Di Baldassarre, G., Bates, P. D., & Brath, A. (2009). Optimal corss-sectional spacing in Preissmann Scheme 1D hydrodynamic models. *Journal of Hydraulic Engineering*, 135(2), 96-105. DOI: 10.1061/(ASCE)0733-9429(2009)135:2(96)

Chow, V. T. (1959). *Open-channel hydraulics*. New York: McGraw-Hill.

Cobby, D. M., Mason, D. C., Horritt, M. S., & Bates, P. D. (2003). Two-dimensional hydraulic flood modelling using a finite-element mesh decomposed according to vegetation and topographic features derived from airborne scanning laser altimetry. *Hydrological Processes*, 17, 1979-2000. DOI: 10.1002/hyp.1201

Cook, A., & Merwade, V. (2009). Effect of topographic data, geometric configuration and modeling approach on flood inundation mapping. *Journal of Hydrology*, 377, 131-142. DOI: 10.1016/j.jhydrol.2009.08.015

Das, B. M. (2006). *Principles of geotechnical engineering* (6th ed.). Australia: Thomson.

De Doncker, L., Troch, P., Verhoeven, R., Bal, K., Meire, P., & Quintelier, J. (2009). Determination of the Manning roughness coefficient influenced by vegetation in the river Aa and Biebrza. *Environmental Fluid Mechanics*, 9, 549-567. DOI 10.1007/s10652-009-9149-0

Densmore, R. V., & Karle, K. F. (2009). Flood effects on an Alaskan stream restoration project: The value of long-term monitoring. *Journal of the American Water Resources Association*, 45(6), 1424-1433. DOI: 10.1111/j.1752-1688.2009.00373.x

Di Baldassarre, G., & Montanari, A. (2009). Uncertainty in river discharge observations: A quantitative analysis. *Hydrology and Earth System Sciences*, 13, 913-921.

Downs, P. W., & Kondolf, G. M. (2002). Post-project appraisals in adaptive management of river channel restoration. *Environmental Management*, 29(4), 477-496. DOI: 10.1007/s00267-001-0035-X

Dudley, R. K., & Platania, S. P. (1997). *Habitat use of the Rio Grande silvery minnow*. Albuquerque, NM: University of New Mexico.

Dudley, R. K., & Platania, S. P. (2007). Flow regulation and fragmentation imperil pelagic-spawning riverine fishes. *Ecological Applications*, 17(7), 2074-2086.

Environmental Systems Research Institute, Inc. (2009). ArcGIS Desktop 9.3 Help. Retrieved from http://webhelp.esri.com/arcgisdesktop/9.3/index.cfm

Federal Emergency Management Agency. (2010). *Flood insurance study, Valencia County, New Mexico* (Flood Insurance Study Number 35061CV000A). Retrieved from http://map1.msc.fema.gov/idms/IntraView.cgi?KEY=92089374&IFIT=1

French, J. R. (2003). Airborne LiDAR in support of geomorphological and hydraulic modelling. *Earth Surface Processes and Landforms*, 28, 321-335. DOI: 10.1002/esp.484

Getis, A., & Ord, J. K. (1992). The analysis of spatial association by use of distance statistics. *Geographical Analysis*, 24(3), 189-206.

Glenn, E. P., & Nagler, P., L. (2005). Comparitive ecophysiology of Tamarix ramosissima and native trees in western U.S. riparian zones. *Journal of Arid Environments*, 61, 419-446.

Goble, D. D., Scott, J. M., & Davis, F. W. (2005). *Endangered species act at thirty, Vol. 1: Renewing the conservation promise*. Island Press: Washington, D. C.

Hatch, M. D., & Gonzales, E. (2010). *Los Lunas habitat restoration fisheries monitoring 2009* (SWCA Project No. 15009). Albuquerque, NM: United States Department of the Interior, Bureau of Reclamation.

Ho, J., Coonrod, J., Gill, T., & Mefford, B. (2010). Case study: Movable bed model scaling for bed load sediment exclusion at intake structure on Rio Grande. *Journal of Hydraulic Engineering*, 136(4), 247-250. DOI: 10.1061/(ASCE)HY.1943-7900.0000149

Horritt, M. S., & Bates, P. D. (2002). Evaluation of 1D and 2D numerical models for predicting river flood inundation. *Journal of Hydrology*, 268, 87-99.

Hsieh, P., & Bolton, S. (2007). Laminar surface water flow over vegetated ground. *Journal of Hydraulic Engineering*, 133(3), 335-341. DOI: 10.1061/(ASCE)0733-9429(2007)133:3(335)

Isaacson, K. (2009). Modeling riparian groundwater depth as a function of river flow for the Rio Grande at Albuquerque, NM. (Master's thesis). Retrieved from http://hdl.handle.net/1928/9346

Jowett, I. G. (2003). Hydraulic constraints on habitat suitability for benthic invertebrates in gravel-bed rivers. *River Research and Applications*, 19, 495-507. DOI: 10.1002/rra.734

Khoury, F. (2005). History of the Manning formula. Retrieved from San Diego State University website: http://manning.sdsu.edu

Kondolf, G. M., & Micheli, E. R. (1995). Evaluating stream restoration projects. *Environmental Management*, 19(1), 1-15.

Le Coarer, Y. (2007). Hydraulic signatures for ecological modeling at different scales. *Aquatic Ecology*, 41, 451-459.

Leon, C., Julien, P. Y., & Baird, D. C. (2009). Case study: Equivalent widths of the Middle Rio Grande, New Mexico. *Journal of Hydraulic Engineering*, 135(4), 306-315. DOI: 10.1061/(ASCE)0733-9429(2009)135:4(306)

Lesica, P., & Miles, S. (2004). Ecological strategies for managing tamarisk on the C.M. Russell National Wildlife Refuge, Montana, USA. *Biological Conservation*, 119, 535-543.

Lobb, M. D., & Orth, D. J. (1991). Habitat use by an assemblage of fish in a large warmwater stream. *Transactions of the American Fisheries Society*, 120, 65-78.

Marks, K., & Bates, P. (2000). Integration of high-resolution topographic data with floodplain flow models. *Hydrological Processes*, 14, 2109-2122.

Marsh, N. A., Western, A. W., & Grayson, R. B. (2004). Comparison of methods for predicting incipient motion for sand beds. *Journal of Hydraulic Engineering*, 130(7), 616-621. DOI: 10.1061/(ASCE)0733-9429(2004)130:7(616)

McLean, S. R., Wolfe, S. R., & Nelson, J. M. (1999). Predicting boundary shear stress and sediment transport over bed forms. *Journal of Hydraulic Engineering*, 125(7), 725-736.

Merwade, V., Olivera, F., Arabi, M., Edleman, S. (2008). Uncertainty in flood inundation mapping: Current issues and future directions. *Journal of Hydraulic Engineering*, 13,(7), 608-620. DOI: 10.1061/(ASCE)1084-0699(2008)13:7(608)

Merwade, V. (2009). Effect of spatial trends on interpolation of river bathymetry. *Journal of Hydrology*, 371, 169-181. DOI: 10.1016/j.jhydrol.2009.03.026

Munson, B. R., Young, D. F., & Okiishi, T. H. (2006). *Fundamentals of fluid mechanics* (5th ed.). Hoboken, NJ: John Wiley & Sons, Inc.

New Mexico Office of the State Engineer. (2010). *Rio Grande Compact*. Retrieved from: http://www.ose.state.nm.us/PDF/ISC/ISC-Compacts/Rio_Grande_Compact.pdf

New Mexico State University. (2010). Climate of New Mexico. Retrieved from: http://weather.nmsu.edu/News/climate-in-NM.htm

Noman, N. S., Nelson, E. J., & Zundel, A. K., (2001). Review of automated floodplain delineation from digital terrain models. *Journal of Water Resources Planning and Management*, 127(6), 394-402.

Nordin, C. F. (1964). *Aspects of flow resistance and sediment transport, Rio Grande near Bernalillo, New Mexico* (Water-Supply Paper 1498-H). http://onlinepubs.er.usgs.gov/djvu/WSP/wsp_1498.djvu

Nordin, C. F. & Beverage, J. P. (1965). *Sediment transport in alluvial channels: Sediment transport in the Rio Grande New Mexico* (Professional Paper 462-F). Retrieved from United States Geological Survey website: http://onlinepubs.er.usgs.gov/djvu/PP/pp_462_f.djvu

Omer, C. R., Nelson, E. J., & Zundel, A. K. (2003). *Journal of the American Water Resources Association*, 39(2), 467-475.

Poff, N. L., Allan, J. D., Bain, M. B., Karr, J. R., Prestegaard, K. L., Richter, B. D., Sparks, R. E., & Stromberg, J. C. (1997). The natural flow regime. *BioScience*, 47(11), 769-784.

Rood, S. B., & Mahoney, J. M. (1990). Collapse of riparian poplar forests downstream from dams in western prairies: Probable causes and prospects for mitigation. *Environmental Management*, 14(4), 451-464.

Sarmiento, O. A., & Falcon, M. A. (2006) Critical bed shear stress for unisize sediment. *Journal of Hydraulic Engineering*, 132(2), 172-179. DOI: 10.1061/(ASCE)0733-9429(2006)132:2(172)

Schumann, G., Matgen, P., Cutler, M. E. J., Black, A., Hoffman, L., Pfister, L. (2008). Comparison of remotely sensed water stages from LiDAR, topographic contours and SRTM. *ISPRS Journal of Photogrammetry & Remote Sensing*, 63, 283-296. DOI: 10.1016/j.isprsjprs.2007.09.004.

Scurlock, D. (1998). *From the Rio to the Sierra: An environmental history of the Middle Rio Grande Basin* (General Technical Report RMRS-GTR-5). Fort Collins, CO: United States Department of Agriculture, Forest Service.

Shaforth, P. B., Stromberg, J. C., & Patten, D. T. (2002). Riparian vegetation response to altered disturbance and stress regimes. *Ecological Applications*, 12(1), 107-123.

Shatnawi, F. M., & Goodall, J. L. (2010). Comparison of flood top width predictions using surveyed and LiDAR-derived channel geometries. *Journal of Hydraulic Engineering*, 15(2), 97-106. DOI: 10.1061/(ASCE)HE.1943-5584.0000161

Shields, F. D., Cooper, C. M., Knight, S. S., & Moore, M. T. (2003) Stream corridor restoration research: A long and winding road. *Ecological Engineering*, 20, 441-454. DOI:10.1016/j.ecoleng.2003.08.005

Spiegel, M. R., Schiller, J. J., & Srinivasan, R. A. (2000). *Schaum's outline of theory and problems of probability and statistics*. New York: McGraw-Hill.

Siegle, R., & Reed, G. (2007). *2006 monitoring report for the Los Lunas habitat restoration site*. Denver, CO: U.S. Department of the Interior, Bureau of Reclamation.

Simmons, M. (1988). *New Mexico: An interpretive history.* Albuquerque: University of New Mexico Press.

Slaugh, D. (2003). *Los Lunas habitat restoration project post-construction summary report*. Albuquerque, NM: United States Department of the Interior, Bureau of Reclamation.

Stanford Environmental Law Society. (2000). A brief history of the endangered species act. In P. S. Easley, J. P. Holtman, J. Scancarelli, & B. A. Schmidt (Eds.), *The Endangered Species Act*. (p. 18). Stanford, CA: Stanford University Press.

Statzner, B., Gore, J. A., & Resh,V. H. (1988). Hydraulic stream ecology: observed patterns and potential applications. *Journal of the North American Benthological Society*, 7(4), 307-360.

Stephan, U., & Gutknecht, D. (2002). Hydraulic resistance of submerged flexible vegetation. *Journal of Hydrology*, 269, 27-43.

Sturm, T. W. (2010). *Open channel hydraulics*. New York: McGraw-Hill.

Udall, S. L. (1967). Native Fish and Wildlife Endangered Species. *Federal Register*, 32(48), 4001.

United States Department of Agriculture, Natural Resource Conservation Service. (2010a). Plant fact sheet: Eastern cottonwood. Retrieved from website: http://plants.usda.gov/factsheet/pdf/fs_pode3.pdf

United States Department of Agriculture, Natural Resource Conservation Service. (2010b). Plant guide: Coyote willow. Retrieved from website: http://plants.usda.gov/plantguide/pdf/cs_saex.pdf

United States Department of Agriculture, Natural Resource Conservation Service. (2010c). Plant profile: Tamarix ramosissima Ledeb. Retrieved from website: http://plants.usda.gov/java/profile?symbol=TARA

U.S. Department of the Interior, Fish and Wildlife Service. (2002). *Final recovery plan for the Southwestern willow flycatcher*. Retrieved from http://ecos.fws.gov/docs/recovery_plans/2002/020830c.pdf

U.S. Department of the Interior, Fish and Wildlife Service. (2003). Endangered and threatened wildlife and plants; designation of critical habitat for the Rio Grande silvery minnow final rule. *Federal Register*, 68(33), 8087-8135.

U.S. Department of the Interior, Fish and Wildlife Service. (2005). Endangered and threatened wildlife and plants; designation of critical habitat for the southwestern willow flycatcher (Empidonax traillii extimus). *Federal Register*, 70(201), 60885-60934.

U.S. Department of the Interior, Fish and Wildlife Service. (2009). *ESA basics: More than thirty years of conserving endangered species*. Retrieved from website: http://www.fws.gov/endangered/factsheets/ESA_basics.pdf

U.S. Department of the Interior, Fish and Wildlife Service. (2010a). Rio Grande silvery minnow (Hybognathus amarus) recovery plan, first revision. Retrieved from website: http://ecos.fws.gov/docs/recovery_plan/022210_v2.pdf

U.S. Department of the Interior, Fish and Wildlife Service. (2010b). *Species Reports*. Retrieved from website: http://ecos.fws.gov/tess_public

U.S. Department of the Interior, Geological Survey. (2010a). *USGS 08313000 Rio Grande at Otowi Bridge, near San Ildefonso, NM Water Data Report, 2009*. Retrieved from website: http://wdr.water.usgs.gov/wy2009/pdfs/08313000.2009.pdf

U.S. Department of the Interior, Geological Survey. (2010b). "USGS 08313000 Rio Grande at Otowi Bridge, near San Ildefonso, NM." *National Water Information System*. Retrieved from website: http://waterdata.usgs.gov/nwis/uv? 08313000

U.S. Department of the Interior, Geological Survey. (2010c). *USGS 08330000 Rio Grande at Albuquerque, NM Water Data Report, 2009*. Retrieved from USGS website: http://wdr.water.usgs.gov/wy2009/pdfs/08330000.2009.pdf

U.S. Department of the Interior, Geological Survey. (2010d). "USGS 08330000 Rio Grande at Albuquerque, NM." *National Water Information System*. Retrieved from website: http://waterdata.usgs.gov/nwis/uv?08330000

U.S. Department of the Interior, Geological Survey. (2010e). *USGS 08331160 Rio Grande near Bosque Farms, NM Water Data Report, 2009*. Retrieved from USGS website: http://wdr.water.usgs.gov/wy2009/pdfs/08331160.2009.pdf

U.S. Department of the Interior, Geological Survey. (2010f). "USGS 08331160 Rio Grande near Bosque Farms, NM." *National Water Information System*. Retrieved from website: http://waterdata.usgs.gov/nwis/uv?08331160

Wang, P., Wang, C., & Zhu, D. Z. (2010). Hydraulic resistance of submerged vegetation related to effective height. *Journal of Hydrodynamics*, 22(2), 265-273. DOI: 10.1016/S1001-6058(09)60054-8

Wiberg, P. L., & Smith, J. D. (1987). Calculations of the critical shear stress for motion of uniform and heterogeneous sediments. *Water Resources Research*, 23(8), 1471-1480.